HMG Advance Access published January 6, 2010

PKD1 TRANSGENIC MICE: ADULT MODEL OF POLYCYSTIC KIDNEY DISEASE WITH EXTRARENAL AND RENAL PHENOTYPES

Almira Kurbegovic†[1], Olivier Côté†[1], Martin Couillard[1], Christopher J. Ward[2], Peter C. Harris[2], Marie Trudel*[1]

† both authors contributed equally

[1]Institut de Recherches Cliniques de Montreal, Molecular Genetics and Development, Faculte de Medecine, Universite de Montreal, Montreal, Quebec, Canada [2] Mayo Clinic, Rochester, MN, USA

*Correspondence:
Dr. Marie Trudel
Director, Molecular Genetics and Development
IRCM
110 ave. des Pins ouest,
Montreal, Quebec, Canada, H2W 1R7
Tel: 1-(514) 987-5712
Fax: 1-(514) 987-5585
Email: trudelm@ircm.qc.ca

ABSTRACT

While high levels of Pkd1 expression are detected in tissues of patients with autosomal dominant polycystic kidney disease (ADPKD), it is unclear whether enhanced expression could be a pathogenetic mechanism for this systemic disorder. Three transgenic mouse lines were generated from a Pkd1-BAC modified by introducing a silent tag via homologous recombination to target a sustained wild type genomic Pkd1 expression within the native tissue and temporal regulation. These mice specifically overexpressed the Pkd1 transgene in extrarenal and renal tissues from ~2- to 15-fold over Pkd1 endogenous levels in a copy-dependent manner. All transgenic mice reproducibly developed tubular and glomerular cysts leading to renal insufficiency. Interestingly, $Pkd1_{TAG}$ mice also exhibited renal fibrosis and calcium deposits in papilla reminiscent of nephrolithiasis as frequently observed in ADPKD. Similar to human ADPKD, these mice consistently displayed hepatic fibrosis and ~15% intrahepatic cysts of the bile ducts affecting females preferentially. Moreover, a significant proportion of mice developed cardiac anomalies with severe left ventricular hypertrophy, marked aortic arch distention and/or valvular stenosis and calcification that had profound functional impact. Of significance, $Pkd1_{TAG}$ mice displayed occasional cerebral lesions with evidence of ruptured and unruptured cerebral aneurysms. This $Pkd1_{TAG}$ mouse model demonstrates that overexpression of wildtype Pkd1 can trigger the typical adult renal and extrarenal phenotypes resembling human ADPKD.

INTRODUCTION

Human autosomal dominant polycystic kidney disease (ADPKD) is one of the most prevalent monogenic diseases with an incidence of 1:400 to 1:1000 individuals. It is a multisystemic disorder characterized by numerous bilateral renal epithelial cysts affecting all segments of the nephron. Eventually, progression of these multiple cysts in kidneys leads to renal insufficiency and end-stage renal disease by late mid-age. Extrarenal clinical manifestations are also common with hepatic cysts being the most frequent, and predominately so, in women. Non-cystic features include cardiac and valvular anomalies and, less frequently, intracranial aneurysms (1).

The majority of patients (85-90%) with ADPKD have a mutation in the PKD1 gene. The gene spans 54kb and encodes a very large protein of 4302 amino acids, polycystin-1. Polycystin-1 is a transmembrane protein that has a large N-terminal extracellular domain with a unique combination of motifs and was reported to undergo partial autocleavage at the G-protein coupled receptor proteolytic site (GPS) (2). Polycystin-1 has been implicated in signal transduction, in mechanosensation, and in cell-cell/cell-matrix interactions. Human PKD1 and polycystin-1 expression have been analyzed in normal and ADPKD tissues. PKD1 and polycystin-1 are normally expressed in a wide range of adult tissues including epithelial and non-epithelial cell types (3-8). Interestingly, PKD1 expression is developmentally regulated, particularly in the kidneys. Polycystin-1 has highest levels in fetal life and is readily detected in glomerular and tubular epithelial cells (reviewed in (9) and reference therein). In normal adult kidneys, the RNA transcript and protein levels of polycystin-1 are decreased to lower levels, most notably in the collecting and distal tubules. By contrast, PKD1 expression levels were increased (~2-fold) in ADPKD kidneys (3, 10) and consistently, the majority of renal epithelial cysts displayed persistent or enhanced levels of polycystin-1 (4).

Although ADPKD is a dominant disease, the stochastic nature of the renal cysts in ADPKD suggests that the mutational mechanism for PKD1 could result from a two-hit phenomenon or a loss of heterozygosity. This mechanism is supported by detection of PKD1 clonal somatic mutations in cells from a significant proportion of cysts (11-13). Moreover, loss of heterozygosity could account for the widely varying phenotype commonly observed in individual families. This mechanism would however be at variance with the persistent or enhanced expression of PKD1 seen in the majority of human renal cysts, unless a mechanism of gain-of-function/overexpression may also be operant.

The mouse Pkd1 gene has very close similarities to the human PKD1 and may provide important insights into PKD1 function(s). During normal development, murine Pkd1 is expressed at high levels from the morula stage and detected in all neural crest cell derivatives including adult brain, aortic arch, cartilage, and mesenchymal condensation (14, 15). Homozygous mutant mice targeted for Pkd1 deletion have been reported to develop renal and pancreatic cysts (16-21). These attempts to generate mouse models, unfortunately, did not produce viable animals. Nevertheless, the occurrence of renal cysts in these homozygous Pkd1 mutant mice would be consistent with the hypothesis of a two-hit mutational mechanism in humans that involves a germline mutation and somatic inactivation of the normal allele. This mechanism is also supported by conditional ablation of Pkd1 in mice few days after birth (22) but not upon later ablation since cysts developed only focally (23, 24). However, evidence of a mechanism of haploinsufficiency or gene dosage reduction for cystogenesis was provided in mice homozygous for a Pkd1 hypomorphic allele or heterozygous for a Pkd1 deleted allele (25, 26). Moreover, Pkd1 gain of function may also be an additional mechanism for ADPKD pathogenesis as determined by the renal-targeted Pkd1 in SBPkd1$_{TAG}$ mice with renal cystogenesis (27). These findings would support a gene dosage dependent mechanism for ADPKD where mutations of loss of heterozygosity,

haploinsufficiency, or overexpression could trigger a renal phenotype and thereby provide an explanation for the high penetrance found for a range of different mutations in this disease.

To interrogate increased Pkd1 dosage as an ADPKD pathogenetic mechanism, Pkd1 in the native genomic context purified from a murine BAC was targeted in transgenic mice. We generated three transgenic lines that expressed systemically increase Pkd1 at proportional gene dosage levels in different tissues. These mice not only develop polycystic kidneys and renal failure but also all the prevalent extrarenal manifestations observed in ADPKD patients including liver cysts, cardiac and valvular anomalies as well as the dreadful complication of ruptured intracranial aneurysms. Our study reproduces the first orthologous ADPKD mouse model with the entire spectrum of adult extrarenal and renal phenotypes.

RESULTS

Production of Pkd1$_{TAG}$-BAC by homologous recombination

To investigate the role of Pkd1 overexpression/gain-of-function in renal and extrarenal tissues, we have used a genomic clone containing the entire Pkd1 gene in a BAC vector 129/Sv library that we previously isolated (27). This BAC contains a ~121kb insert with ~37kb of upstream and ~39kb of downstream sequences of the Pkd1 gene including the entire adjacent Tsc2 gene. This Pkd1-BAC was modified by two successive homologous recombination events. First, the Pkd1 gene was tagged in exon 10 by substituting a nucleotide (G to A) to create a novel EcoRI site at position 2355 on the cDNA map. This silent point mutation was produced to readily distinguish the Pkd1 gene and transcript of the BAC from that of endogenous origin. Second, we have deleted the Tsc2 gene (~34.5kb) of the Pkd1-BAC to prevent introducing the Tsc2 gene exogenously and to reduce the BAC size (Figure S1). This new Pkd1$_{TAG}$-BAC was digested with MluI, a unique site located at ~24.8kb upstream of the Pkd1 translation

initiation site, and NotI site in the BAC polylinker sequences to remove the prokaryotic BAC vector sequences (Supplemental Figure 1, Figure 1). This ~75kb MluI-NotI fragment was isolated, purified and quantified for oocytes microinjection (28).

Production and analysis of $Pkd1_{TAG}$ transgenic mice

Three transgenic founders carrying several copies (2 to 15) of the $Pkd1_{TAG}$ transgene as determined by Southern analysis, served to derive three transgenic lines. Characterization of the transgene chromosomal integrity in these lines was performed with 5', internal, and 3' probes (a to g) used for BAC analysis in Supplemental Figure 1. Transgene 5' flanking sequence was monitored for presence of a specific polymorphism from the 129/Sv genetic background by a band at 100bp compared to the 113bp and/or 133bp typical of the inbred C57Bl/6J and CBA/J strains used to produce these transgenic mice (Figure 1). To verify the transgene 3' end, a probe consisting of the Pkd1 gene exon 45-46 was used to detect the endogenous 7.0kb Pkd1 band as well as the transgene 5.0kb (Figure 1). The $Pkd1_{TAG}$ mice contained complete copies of the Pkd1 transgene based also on the internal genomic overlapping structure analysis.

Pkd1 expression in adult $Pkd1_{TAG}$ transgenic mice

Analysis of $Pkd1_{TAG}$ transgene and Pkd1 endogenous gene expression was carried out in several tissues. To first quantify the transcript levels from the transgene comparatively to the endogenous gene, Northern blots were performed on kidneys (n=4) of each transgenic line (Figure 2A). The transgene transcript size was identical to the endogenous transcript of 14.2kb. All $Pkd1_{TAG}$ transgenic mice showed systematically increased transcript Pkd1 levels in kidneys relative to controls. In fact, $Pkd1_{TAG}$ transgene renal expression increased with the number of $Pkd1_{TAG}$ copies (2, 6, 15) in each line compared to controls (n=2): line 6 (n=4), 18 (n=3), 26 (n=3) displayed ~1.9±0.8, 6.0±0.9 and 17.9±1.9 fold increase respectively.

Quantification of transgene expression levels was carried out by real-time PCR in the three transgenic lines at adult age, by using primers in the exon 1 and 2 of Pkd1 (Figure 2B). The $Pkd1_{TAG}$ expression in transgenic mice was compared to S16 ribosomal protein gene product as internal standard. Analysis of Pkd1 renal expression showed similar fold increase for transgenic kidneys as those obtained by Northern blot. Since endogenous Pkd1 expression levels are modulated in various tissues, we quantified $Pkd1_{TAG}$ expression levels to determine whether the transgene followed the endogenous gene expression pattern. Transgene expression by real-time PCR consistently and specifically showed highest expression in the brain of all transgenic lines relative to other organs (Figure 2B). The heart, lung, and brain displayed higher Pkd1 levels than in the kidneys whereas the other organs including spleen, liver, and pancreas levels were lower. Interestingly, the three transgenic lines demonstrated, within all tissues analyzed, a comparable increase in transgene to endogenous expression, indicating that the $Pkd1_{TAG}$ transgene contained all the appropriate regulatory elements for tissue expression.

To monitor whether gene expression correlated with the levels of Pkd1 protein or polycystin-1 (Pc-1), Western blot was performed on various tissues of the $Pkd1_{TAG}26$ line using the 7e12 Pc-1 monoclonal antibody and Gapdh as control. The $Pkd1_{TAG}26$ showed several fold increase of Pc-1 for all extrarenal and renal tissues relative to non-transgenic control mice (Figure 2C). Subsequently, phenotype caused by transgene expression was characterized in the $Pkd1_{TAG}$ mice by gross and histology analysis of tissues frequently affected in human ADPKD.

Renal anomalies in $Pkd1_{TAG}$ mice

$Pkd1_{TAG}$ transgenic adult kidneys of all three lines were generally pale and exhibited bilateral cysts studding the cortical surface. Histologically, transgenic mice developed multiple microscopic and macroscopic cysts affecting cortex and medulla as well as glomerular cysts (Figure 3A-F). Anomalies were detected at 1 month of age for $Pkd1_{TAG}$ 6 and 26 mice as mild tubular dilatation and scattered

tubular microcysts with epithelial hyperplasia respectively, suggesting abnormal features early on as observed in ADPKD patients. The renal phenotype in $Pkd1_{TAG}$ 26 developed much more rapidly than in the $Pkd1_{TAG}$ 6 mice. Consistently, $Pkd1_{TAG}$ 26 kidneys at 2-months had tubular and glomerular cysts that became very severe by 3-months of age whereas $Pkd1_{TAG}$ 6 displayed glomerular and tubular dilatation at 7 months of age that progressed to cysts at 9 months and were severely cystic by 12-16 months of age. Cystic and even non-cystic tubules frequently displayed epithelial hyperplasia and hypertrophy and occasional presence of polyps with variable severity between mice. Hemorrhagic cysts consistent with some hematuria, proteinaceous casts in tubular cysts as well as interstitial fibrosis were commonly observed (Figure 3B). To evaluate levels of fibrosis, we quantified the density of Sirius red staining in $Pkd1_{TAG}$6 (n=6, 7-16months) at 5.7% and 26 kidneys (n=6, 2-8months) at 9.6% that was markedly elevated by ~4.8- and 8-fold respectively compared to controls (n=5; 1.2%). Further, partial and total sclerosis of glomeruli was detected in all three transgenic lines. To define more precisely the origin of the renal cysts, we used specific nephron segment markers of the proximal, distal, and collecting tubules. As shown in Figure 3C and D, cysts originated from all segments of the nephron with highest and similar proportion in proximal and collecting tubules (~30-35%). A significant proportion of cysts (~20%) were unstained, some of which with presence of mesangial tuft could be identified of glomerular origin whereas others could be from undifferentiated tubular epithelial cells. Analysis of $Pkd1_{TAG}$26 mice (7/18) with highly invasive renal cysts also displayed calcium deposits that were mainly localized to the papilla, reminiscent of the renal calculi described frequently in ADPKD (29-31) (Figure 3E versus F). Since we observed the presence of renal epithelial hyperplasia and polyps, we monitored cell proliferation with the nuclear antigen Ki67 marker by immunostaining in $Pkd1_{TAG}$ 6 and 26 lines (Figure 3G, H). Proliferation was calculated as a percentage of tubules with 0, 1 or ≥2 Ki67-positive cells in the kidneys. In control animals, >92% of tubules (n=941) had no Ki67-positive cells and 5.4% or 2.1% of tubules displayed 1 or ≥2 positive cells respectively. By contrast, the $Pkd1_{TAG}$ 26 line displayed 22.6%

and 27.5% of cystic tubules with 1 and ≥2 Ki67 positive cells, a significant increase of 4 to 10-fold relative to controls ($p<0.01$). Similar levels of proliferation were also observed for the $Pkd1_{TAG}$ 6 line (16% and 26% of 1 and ≥2 Ki67 positive cells). To determine whether c-myc is implicated in the $Pkd1_{TAG}$ renal phenotype, c-myc expression was analyzed by real-time PCR and immunohistochemistry. Expression of c-myc was increased by ~4.8-fold in the $Pkd1_{TAG}$ 26 mice (n=4) relative to controls (n=4) (≤0.02). Consistently, renal sections of $Pkd1_{TAG}$ 6 and 26 mouse lines also revealed diffusely elevated levels of c-myc relative to controls and frequently more pronounced nuclear staining in cystic epithelium (Figure 3I, J), suggesting that c-myc could be an indirect effector of $Pkd1_{TAG}$.

Since cilia anomalies have been associated with cyst formation, cilia of renal epithelial cells were monitored by α-acetylated tubulin staining in $Pkd1_{TAG}$ 26 line and control mice at few weeks of age prior to overt cystogenesis (Figure 3K, L). Most strikingly, the cilia size distribution (at 1 μm interval) in all $Pkd1_{TAG}$ mice showed significantly longer cilia length relative to controls (Figure 3L). Indeed, most cilia of the $Pkd1_{TAG}$ mice (n=346) (Figure 3L) were >5 μm whereas cilia in controls (n=266) (Figure 3K) were mainly 2-3 μm in length. Cilia from $Pkd1_{TAG}$ renal epithelium were often of kinky structure and occasionally displayed 2 or multicilia by EM. These mice consistently developed PKD features pointing to the induced expression from the transgene as specifically responsible for the pathogenesis.

Altered renal physiology in $Pkd1_{TAG}$ mice

Renal function was monitored in the low and high expressor $Pkd1_{TAG}$ 6 and 26 transgenic lines. Animals were monitored for urinary levels of urea nitrogen, creatinine, protein, and urine osmolality and volume (Table 1). In comparison to negative controls of same genetic background, the low and high expressors exhibited significant increase in urine volume similar to the positive PKD controls SBM mice (28).

These urinary and blood analysis are consistent with mild concentrating defects but cannot exclude AVP deficiency. Accordingly, urinary urea nitrogen, creatinine, and protein were significantly decreased. In addition, $Pkd1_{TAG}$ mice had urinary calcium (0.8±0.2; n=8, 9-14 months) and urinary pH (6.0±0.1, n=16, 7-18 months) comparable to controls (0.9±0.2; n=4, 11 months) (5.9±0.1, n=4, 11 months). Mice from all three $Pkd1_{TAG}$ lines were also monitored for hematocrit levels since patients with progressive renal insufficiency commonly develop anemia. Consistently, the three $Pkd1_{TAG}$ mouse lines at 5 to 7 months of age displayed significantly reduced hematocrit levels (Table 1 and data not shown). Mice from the three transgenic $Pkd1_{TAG}$ lines were also analyzed qualitatively for proteinuria from urine samples on SDS-PAGE (Figure 4 A). Despite the reduced concentration level of protein in urine, $Pkd1_{TAG}$ animals at 4 months of age appeared to display non-selective proteinuria that was most pronounced in the high transgene expressor. To determine whether Pc-1 in $Pkd1_{TAG}26$ transgenic mice were present in urine, we prepared total crude protein from urine (T), urine devoided of exosome or uromodulin aggregates (supernatant 1, S1), the resuspended pellet was separated in two additional fractions the surpernatant containing uromodulin (supernatant 2, S2) and urinary exosome following the protocol of (32, 33). Western analysis of total crude urinary protein with the LRR Pc-1 antibody (7e12) showed a similar pattern to that of total kidney extracts from native untreated (N) and deglycosylated (DG) samples (Figure 4B). While samples in the native form displayed two protein bands estimated by migration at ~360-380kDa and slightly above ~420kDa, in the deglycosylated form a unique product was detected corresponding to the lower band. Pc-1 was detected in three urine fractions (T, S1, and exosomes) whereas it appears absent in the supernatant (S2) for both control and transgenic mice. In exosomal pellet fraction, Pc-1 was present mainly in the glycosylated form, as observed in human ADPKD urinary exosomes (33). Interestingly, significant proportion of Pc-1 was also found in the S1 supernatant in both $Pkd1_{TAG}$ transgenic mice and controls in both glycosylated and unglycosylated forms, suggesting that the N-terminal domain of Pc-1 is likely excreted in the urine. Importantly, similar fold enrichment in Pc-

1 was observed in Pkd1$_{TAG}$26 transgenic mice relative to controls in all three Pc-1 containing fractions, indicating that the Pc-1 from the transgene follow a normal physiological process.

Hepatic anomalies in Pkd1$_{TAG}$ mice similar to PKD

Since human ADPKD frequently developed biliary dysgenesis, we investigated whether enhanced Pkd1$_{TAG}$ gene expression could induce hepatic abnormalities in mice. Readily from macroscopic liver examination, hepatic cysts could be detected in both transgenic 6 and 26 lines (low and high Pkd1 expressors): 5 of 34 Pkd1$_{TAG}$ transgenic mice from line 26 and in 1 of 32 from line 6 (Figure 5A, B). Histologically, these liver developed cysts likely of cholangiocyte origin that ranged from mild to very severe (Figure 5C, D). Interestingly, these characteristic cystic features affected mainly female mice (4 out of 5) as in human ADPKD. Further, hepatic parenchyma from both transgenic 6 and 26 lines showed presence of a broad band of fibrosis along the intrahepatic ducts that was systematically observed and in some mice, fibrosis was widespread (Figure 5E, F). Quantification of fibrosis over the liver sections showed ~4- to 5-fold increased respectively for the Pkd1$_{TAG}$ 6 (9.8±9.3%; n=10; $p \leq 0.02$) and 26 lines (11.1±7.9%; n=12; $p < 0.002$) compared to controls (1.9±0.8%; n=10). Similar to Pkd1$_{TAG}$ 6 and 26 renal analysis, we evaluated whether proliferation could be implicated in the hepatic cysts, liver sections were stained with Ki67. The epithelial linings of cysts were uniformly delineated by enhanced Ki67 staining and/or by strong nuclear staining (Figure 5G, H). These Pkd1$_{TAG}$ livers also displayed elevated c-myc expression in the cystic areas with more intense signal in cell lining the cysts (Figure 5I, J). Interestingly, this increased proliferation and myc expression paralleled the marked fibrosis in regions of liver cysts. Since the Pkd1$_{TAG}$ 6 and 26 transgenic mice develop typical hepatic ADPKD characteristics, it is likely that Pkd1 overexpression in the liver may be a pathogenetic mechanism through potentially modulating c-myc.

Cardiac anomalies in Pkd1$_{TAG}$ mice

Because a proportion of ADPKD patients develop cardiac anomalies, we performed physiologic studies using non-invasive ultrasound imaging in Pkd1$_{TAG}$ 6 and 26 relative to control mice (Figure 6A, B; Table 2). The M-mode dimensions showed significantly increased left ventricular posterior wall thickness at diastole and at systole indicating left ventricular hypertrophy (Table 2A). The interventricular septa thickness was also increased. Further, the aortic root diameter and area were significantly increased in the Pkd1$_{TAG}$ mice showing important dilatation as described in ADPKD patients. At necropsies, gross heart anatomy of mice from the three Pkd1$_{TAG}$ lines showed significant and extensive enlargement relative to that of negative control littermates (Figure 6C, D; Table 2A), providing evidence of eccentric dilated cardiac hypertrophy. Hearts of Pkd1$_{TAG}$ relative to controls also showed important alteration in the cardiac structure and morphology as analyzed by Microfil casting that fills the body entire vasculature providing a three-dimensional visualization of organ circulation (Figure 6E, F). Substantial abnormalities of the ventricular vasculature were readily detectable under different angles, suggesting injury to the myocardium with possible development of fibrosis (Figure 6F vs E). We then verified by histology and detected that 35-40% of Pkd1$_{TAG}$ mice (lines 18 and 26) displayed to 2-to 4-fold increase in cardiac fibrosis.

Functional analysis by echographic measurements consistently showed a marked increased in stroke volume as well as in the cardiac output by almost 2-fold in Pkd1$_{TAG}$26 mouse lines (Table 2B). While the heart rates of Pkd1$_{TAG}$ and control mice were similar, cardiac valves displayed some anomalies in the Pkd1$_{TAG}$ mice (Table 2B) (Figure 6A, B). As shown in Table 2, the significant increase in mean and peak velocity downstream of the aortic valve suggested stenosis. This increased velocity measurement was consistent with the abnormal aortic valve leaflets detected by ultrasound imaging as opaque in some Pkd1$_{TAG}$ 6 and 26 mice rather than delicate and translucent (Figure 6B). Upon heart sectioning, large

areas within the ventricular lining exhibited change in pigmentation, indicative of ventricular lining calcification (Figure 6G, H). To determine whether the valves opacity and ventricular lining anomalies resulted from calcium deposits, cardiac histologic sections were stained individually with Alizarin and VonKossa. Analysis revealed presence of calcification in 6 of the 15 aortic valves, 4 of which also had staining in ventricular lining (Figure 6I, J). Furthermore, 3 of these 6 $Pkd1_{TAG}$ mice exhibited staining in the myocardium as well. Since observations of valvular, vascular, and myocardium calcification in individuals with chronic kidney disease has been associated with higher serum phosphate (34), we determined the levels of phosphate in serum of $Pkd1_{TAG}$ mice. Analogously to human, the $Pkd1_{TAG}$ mice (1.9±0.3 mmol/L; n=8) had significantly increased serum phosphate relative to controls (1.4±0.2 mmol/L; n=4), supporting the hypothesis that elevation in serum phosphate concentration may contribute to calcification risk and cardiovascular events.

Vascular anomalies in $Pkd1_{TAG}$ mice

To investigate whether adult $Pkd1_{TAG}$ mouse lines exhibited altered cardiovascular response, we measured blood pressure in two $Pkd1_{TAG}$ lines (26 and 18) and control mice using the tail cuff method. Two groups of $Pkd1_{TAG}$ mice were readily distinguishable in both lines. In $Pkd1_{TAG}$26 line (6-7 months of age), the first group of mice (n=5) exhibited systolic blood pressure at 113.5±11.0 mmHg comparable to control mice (n=4) of systolic blood pressure at 116.2± 3.1 mmHg. The second group of $Pkd1_{TAG}$ 26 mice (n=3) had significantly increased blood pressure at 161.1±5.1 mmHg ($p<0.001$). Similarly, evidence of hypertension in two of six $Pkd1_{TAG}$18 mice (132.3±1.3 mmHg; $p<0.0009$) indicated that the $Pkd1_{TAG}$ mouse lines can progress to severe hypertension as in human ADPKD.

Upon signs of distress in three mice of $Pkd1_{TAG}$ 26 line, we macroscopically observed severe hemorrhage and severe intracranial edema. These mice at dissection did not show closure of the cranial

bone at the sutura sagitalis and have evidence of hydrocephalus with ventricle dilatation (Figure 7A and B). No control mice exhibited this phenotype. In the $Pkd1_{TAG}$ 26 mice, subarachnoid hemorrhages were observed in different areas of the brain and were so severe in some cases that a significant portion of the brain was completely destroyed/obliterated. Further, the cerebellum of these $Pkd1_{TAG}$ 26 mice at histologic examination was underdeveloped, reduced in size or constricted, providing signs of prior compression of this region and adjacent structures (Figure 7D). To visualize and analyze the vasculature, we introduced Microfil casting to model the entire vasculature of $Pkd1_{TAG}$ 26 (n=5) and control (n=7) mice. As illustrated in Figure 7E-F, two $Pkd1_{TAG}$26 mice compared to none in controls showed unruptured cerebral aneurysm, the most dreadful complication of ADPKD.

Lifespan in $Pkd1_{TAG}$ mice

Lifespan of mice from the three transgenic $Pkd1_{TAG}$ lines was also quantified. Animals died at 5.5 ± 2.8 months (n=18) for the high expressing $Pkd1_{TAG}$ 26 line presumably due at least in part to renal failure, at older age of 16.7±5.5 months (n=9) and 16.6±1.8 months (n=12) for the lower expressors $Pkd1_{TAG}$ 18 and 6 lines respectively.

DISCUSSION

This study reports generation and characterization of the first Pkd1 mouse model of ADPKD that develops the typical renal and extrarenal pathologic spectrum. This model was produced by expressing a "wild type" full length Pkd1 gene and proximal regions purified from a BAC that produces a functional polycystin-1 (Pc-1) protein. Since this mouse model reproduces both the entire phenotypic spectrum and at the similar frequency occurrence as in ADPKD, a systemic Pkd1 enhanced expression is most likely a pathogenetic mechanism.

The three transgenic $Pkd1_{TAG}$ mouse lines generated showed a copy-number dependent expression of the full-length Pkd1 transgene in all tissues. Since the regulatory pattern of transgene expression was similar to that of the endogenous gene, it is likely that the transgene includes all the necessary transcriptional regulatory regions of the Pkd1 gene. Consistently, the Pc-1 protein is also similarly overexpressed in these mice. Of importance, gene dosage or expression correlated with the progression of phenotypic severity.

The $Pkd1_{TAG}$ mice are the first model among the mice with dysregulated or mutated Pkd1 gene that develops the typical multicystic "bosselated" cortical surface with tubular and glomerular cysts as in ADPKD. Renal insufficiency was detected in $Pkd1_{TAG}$ mice at 5-6 months of age by altered urinary and blood analysis. Severe cystogenesis with loss of renal function and increase kidney fibrosis are hallmarks of ADPKD renal pathology. In addition to frequent hemorrhagic cysts and hematuria, an incidence of ~39% of $Pkd1_{TAG}$ mice with pronounced cystic disease displayed intraluminal but also parenchymal calcium deposits limited to the papilla. Presence of this localized nephrocalcinosis in $Pkd1_{TAG}$ mice is compatible with the nephrolithiasis observed in 20-36% of patients with ADPKD (30, 31). While the mechanism responsible for these calcium deposits is unknown, the urinary concentration defect should in theory have a protective effect but urinary stasis within the distorted anatomy and compressed tubules may predispose to calcium precipitation.

Of particular interest was the significantly longer primary cilium of renal epithelial cells in $Pkd1_{TAG}$ prior to cyst appearances. This indicated that increased expression of normal functional polycystin-1 protein might promote ciliogenesis. Since endogenous Pc-1 was localized to the cilia (35), this finding suggests that it can occur via a direct effect of Pc-1 overexpression and/or through indirect Pc-1 cellular effectors modulating proteins of the cilia and axoneme assembly. Since cilia anomalies preceded

cystogenesis, it raises the question whether it is a prerequisite for cyst formation in $Pkd1_{TAG}$ mice. In addition, the increased cilia length distribution also persisted during cystogenesis and this, in spite of significantly elevated renal epithelial proliferation. While defects in the primary cilia have been observed in other cystic diseases, most of cilia anomalies have been attributed to shorter or absence of cilia (35-38) except for the Nek8 and p75/cux genes (39, 40).

The consistent increase in Pc-1 in equivalent proportion from crude urine to subfractionated exosomes of the $Pkd1_{TAG}$ over control mice argues that Pc-1 in transgenic kidneys undergoes the normal *in vivo* physiologic protein processing. The shed Pc-1 protein both glycosylated and unglycosylated in crude urine corresponded approximately in size to a N-terminal cleaved form of Pc-1 at the G protein-coupled receptor proteolytic site (GPS at aa 3041). Strikingly, similar size Pc-1 glycosylated and unglycosylated forms were free in urine itself whereas only the glycosylated form was detected in the exosome fraction. This finding is consistent with the cleaved form of PC-1 present in human urinary exosomes (33, 41). While the role of Pc-1 in exosomes remains to be elucidated, we speculate that the increased frequency of interaction between free Pc-1, exosome and cilia in flow of $Pkd1_{TAG}$ mice could influence intercellular and intracellular signaling. Alternatively, exosomes if in close proximity of cilia as shown *in vitro* (33) could interact, fuse and consequently, induce longer cilia with profound impact on mechanosignaling and tubular integrity.

The spectrum of extrarenal phenotypes in the $Pkd1_{TAG}$ mice closely recapitulates that of human ADPKD. Indeed, the high frequency of hepatic cysts in $Pkd1_{TAG}$ mice affecting mainly females is reminiscent of ADPKD. Cysts affecting intrahepatic bile ducts are consistent with the endogenous pattern of Pkd1 expression (14, 16) and likely due to enhanced transgene expression in $Pkd1_{TAG}$ mice. The systematic increased fibrosis surrounding the biliary ducts in $Pkd1_{TAG}$ mice indicated that fibrosis precedes cyst formation. Furthermore, it also suggests that Pkd1 overexpression interferes with the extracellular

environment and results in active remodeling of the extracellular matrix. Regions of hepatic cysts and fibrosis were associated with elevated proliferation. Interestingly, such association of liver fibrosis and cyst development has also been observed when Pkd1 gene dosage expression is reduced from a hypomorphic allele (42).

The concomitant features of fibrosis and cyst formation in the liver and in kidneys of $Pkd1_{TAG}$ mice correlated with substantial stimulation of proliferation. Such phenotypic similarities to the SBM transgenic mice (43) produced by targeted c-myc expression prompted analysis of c-myc expression in liver and kidneys of $Pkd1_{TAG}$ mice. This study demonstrates that Pkd1 overexpression activates c-myc in both tissues and with a higher signal in cysts. Hence, it is likely a critical component of this signaling event. While the molecular mediators immediately downstream of Pkd1 protein are not yet delineated, c-myc appears to play a central role in the signaling pathway cascade triggered by Pkd1.

Cardiovascular anomalies are the most prevalent non-cystic extrarenal manifestation of ADPKD and of $Pkd1_{TAG}$ mice. $Pkd1_{TAG}$ mice structural cardiac defects are consistent with enhanced Pkd1 transgene expression following the Pkd1 endogenous pattern. We and others have shown that endogenous Pkd1 expression was high in the aortic arch, valve leaflets, atrioventricular cushion, and low in myocardium of wild type mice (8, 14-16, 44). Accordingly, the generalized cardiac anomalies in $Pkd1_{TAG}$ transgenic mice included frequent left ventricular hypertrophy, thickening of the myocardial wall associated with significantly increased aortic root dilatation. In addition, the cardiac aortic and mitral valve morphologic anomalies, particularly stenosis and calcification revealed severe functional impact and suggested signs of valvular regurgitation. In fact, this would be consistent with a compensatory mechanism of heart dilatation/cardiomegaly and increased cardiac output with similar heart rate. In parallel to these anomalies, systemic hypertension in $Pkd1_{TAG}$ mice could be responsible indirectly for the marked aortic

insufficiency as well as the cardiac hypertrophy. However, the strong Pkd1 expression in the aortic valve and root is likely to have a direct contributory role. Together, these cardiac and aortic anomalies with important complications are analogous to those of ADPKD patients (45, 46).

Probably the most devastating extrarenal manifestation in ADPKD is intracranial aneurysm. Given that Pkd1 is expressed in endothelial cells and vascular smooth muscle (8, 47), the presence of cerebral aneurysms in $Pkd1_{TAG}$ was consistent with a primary defect in vascular structure. Similarly, this Pc-1 expression may also be the cause of hypertension independently of renal cystogenesis. Development of cerebral aneurysms in $Pkd1_{TAG}$ mice as in humans is asymptomatic and could be exacerbated by systemic hypertension. However, rupture of aneurysms was detected in a few $Pkd1_{TAG}$ mice at one month of age upon very brief exposure, if any, to hypertension. Rupture of cerebral aneurysms was evident by compression of adjacent structures, focal brain ischemia, and subarachnoid hemorrhage as well as by morbidity.

Systemic enhanced expression of $Pkd1_{TAG}$ mice leads to abnormalities in various organs/tissues as well as in kidneys. Anomalies in a particular organ of $Pkd1_{TAG}$ mice likely result from direct expression of Pkd1 in this organ per se. Evidence for this direct effect instead of a secondary consequence of renal defects, is provided by the renal-targeted Pkd1 mice, $SBPkd1_{TAG}$, that essentially displays a renal restricted PKD disorder (27) similar to that of $Pkd1_{TAG}$ kidney phenotype.

The mutational mechanism of ADPKD was initially proposed as a two-hit model for cyst formation and thereby could explain the focal nature of cyst and the disease variable severity. However, this mechanism is at variance with the continuing expression of PKD1/PC-1 in the majority of ADPKD renal cysts (3-5, 10, 48-50), hepatic cysts (6, 44, 51), and cerebral aneurysms (47). A more inclusive model

would be that an imbalance or dysregulated PKD1/PC-1 would be sufficient to elicit a cystic phenotype. This model is supported by the increase in disease severity correlating with the increase Pkd1 gene dosage in $Pkd1_{TAG}$ and $SBPkd1_{TAG}$ mice (27, 52) and reciprocally with the progressive decrease in expression from haploinsufficiency to hypomorphic Pkd1 allele in mice (23, 25, 42, 53). In fact, both human ADPKD and murine Pkd1 studies have provided evidence for, although opposite, gain-of-function as well as loss-of-function and haploinsufficiency/dosage effect as pathogenetic mechanisms. Hence, a Pkd1 dose imbalance model mechanism would be compatible with a dominantly inherited mutation as seen in humans and could also explain the high prevalence of ADPKD in the population. Importantly, the cystic focal nature in our $Pkd1_{TAG}$ study as in human ADPKD, supports a pathogenetic mechanism that combines Pkd1 dysregulation with an additional mutational step or stochastic event/threshold level to determine whether a cell will enter a cystic cascade and develop cystogenesis.

This study demonstrates that "wild type" full-length Pkd1 overexpression/gain-of-function in the $Pkd1_{TAG}$ mouse is sufficient to reproduce the ADPKD systemic clinical manifestations. Enhanced Pkd1 gene expression recapitulates a physiologic bona fide murine ADPKD disorder with renal and extrarenal phenotypes. Thus, these transgenic mice may be instrumental for numerous studies including the design of novel therapeutic strategies to modulate in vivo progression of ADPKD.

MATERIALS AND METHODS

Constructs for homologous recombination of Pkd1-BAC clone

The Pkd1-BAC clone from the bacterial host strain DH10B ($RecA^-$; $RecBC^+$) was isolated from a 129/Sv mouse pBelo11BAC library (Research Genetics) and was orthologous to the human PKD1 gene as described in (27). To modify the original wild-type Pkd1-BAC by homologous recombination, two constructs were produced in the pLD53.SC-AB BAC recombination vector (54). The first construct was carried out in order to introduce a silent point mutation by substitution of a G to A nucleotide as we did for $SBPkd1_{TAG}$ (27). This substitution created a new EcoRI restriction site in Pkd1 exon 10 that distinguished the transgene from the endogenous gene/transcript. The second construct was performed to delete Tsc2 gene body and consisted of two homology arms, the Tsc2 promoter-intron 2 linked directly to Tsc2 exon 42-exon 46 Pkd1 in a BAC recombination vector. The first homology arm was obtained by PCR amplification of 1116bp fragment (Tsc2 promoter-intron2) with the primers: 5'-TCAGATGCTGCGGCCCGGGACGCA-3' (forward Tsc2 promoter) and 5'-GGACAGCATGCCCTATGCAGATG (reverse intron2) followed by a restriction enzyme digest SmaI-SpHI. The second arm was also generated from a PCR product of 1.2kb with the following primers: 5'-TTCAGCACATGCTCATGCC-3' (reverse Tsc2 intron 40) and 5'-GCTGAAAATGGGCCCATTGTTACC-3' (forward Pkd1 exon 46) followed by a SpHI- BamHI restriction digest that produce 0.9kb from Tsc2 exon42 to exon46 Pkd1. Both these arms were introduced into the pLD53.SC-AB BAC recombination vector.

Modification of BAC clones by homologous recombination in E. coli

Each of the two BAC recombination vectors was used in a two-step RecA strategy for BAC modifications, as previously described (27). Approximately 64 co-integrates were analyzed for each recombination by Southern blot to monitor for appropriate integration event. Two proper co-integrates

were chosen for the second recombination event and positive clones from the resolved BACs were further analyzed by Southern following standard and PFGE using seven probes spanning the entire sequence of the modified BAC. The probes were designed in (14, 27): a. genomic exon 1, b. genomic exon 2-3, c. genomic exon 7-15, d. cDNA exon 15-20, e. cDNA exon 25-34, f. cDNA exon 36-45, g. genomic exon 45-46. Subsequently, modified Pkd1 gene regions were sequenced to confirm that the intended recombined BAC clones were achieved. Following these two modifications the BAC clone was referred as $Pkd1_{TAG}$-BAC.

Production and analysis of $Pkd1_{TAG}$-BAC transgenic mice

The $Pkd1_{TAG}$-BAC (40-50 μg of DNA) was digested with the restriction enzymes MluI and NotI. The ~75kb transgene fragment was isolated on low melt agarose by PFGE. The $Pkd1_{TAG}$ linearized DNA fragment was purified as in (27). The fragment preparation was verified for integrity by PFGE and was microinjected as described (28). Transgenic founder mice and progenies were identified by Southern analysis of DNA from tail biopsies digested with HindIII, EcoRI and/or KpnI and respectively hybridized with the 7 mouse Pkd1 probes to verify integrity of the transgene. The 5' transgene integrity was verified by a polymorphism at 4.47 kb of the murine Pkd1 gene specific for 129/sv that can be distinguished from the C57BL/6J and CBA/J inbred strains that served to produce the transgenic mice. PCR amplification of genomic DNA from transgenic mice at the polymorphic region was carried out with the primers: (forward) 5'-CTGCACCCATGTCAGGTGTA-3' and (reverse) 5'-GTTCTAGGCCAGCCAACTC-3' and expected fragment for 129sv, C57Bl6/J and CBA/J are 100bp, 133bp, and 113bp respectively. All transgenic mouse lines were backcrossed onto C57Bl6/J. Animal procedures were approved by the Animal Care Committee of the IRCM and conducted according to the guidelines of the Canadian Council on Animal Care.

RNA expression analysis

Total RNA was extracted from various tissues, including kidneys, lungs, spleen, brain, heart, pancreas and liver, of 4 to 9 month old animals using guanidium thiocyanate or trizol/chloroform method (55). The integrity of all RNA preparations was monitored by electrophoresis on formaldehyde-agarose gels prior to analysis (56).

$Pkd1_{TAG}$ transgene expression in all tissues was analyzed by quantitative real-time PCR. All RNA samples were reversed transcribed as previously described (10). The primers used were as follows: 5'-TCAATTGCTCCGGCCGCTG- 3' (forward Pkd1 exon 1) and 5'-CCAGCGTCTGAAGTAGGTTGTGGG-3' (reverse Pkd1 exon 2) that detect endogenous and transgene. The S16 ribosomal gene product served as an internal control with the following primers: 5'-AGGAGCGATTT-GCTGGTGTGGA-3' (forward S16 exon 3) and 5'-GCTACCAGGCCTTTGAGATGGA-3' (reverse S16 exon 4). Each pair of primers was designed such that only spliced mRNA would produce the predicted amplification products of 101bp for Pkd1 total (endogenous gene and transgene) and 102bp for S16. All reactions for quantitative real-time PCR analysis were performed in triplicate in a master mix (Qiagen, Mississauga, Canada) using a MX4000 Multiplex quantitative PCR analyser.

Expression analysis of Pkd1 (endogenous gene and transgene) was also performed by Northern blot. Total RNA from each sample (30 μg) was electrophoresed on agarose/formaldehyde gel, transferred to nylon membranes and hybridized with "g" probe for Pkd1 and with glyceraldehyde 3-phosphate dehydrogenase (Gapdh) as internal control (14). Membranes were exposed to X-ray film (Biomax MS) for 24-48 hours, scanned and quantified with the Image Quant 5.0 software.

Protein expression analysis

Total protein extracts from multiple organs, kidney, lung, brain, liver, pancreas and heart, were produced in RIPA buffer (20mM Tris pH8; 2mM EDTA; 150mM NaCl; Triton 0.5%) supplemented by cocktail of inhibitors of proteases (1X, SIGMA) and PMSF (1mM). Protein concentration was measured by Bradford assay (BioRad). Total protein extracts (40 or 80µg) was reduced in NuPAGE loading dye for 7min at 65°C and loaded on 4-12% NuPage Bis-Tris gel using 1X MES SDS Invitrogen migration buffer. Urinary proteins were prepared as described (32, 33). In brief, urine was supplemented with cocktail inhibitors, centrifuged to remove cell debris and supernatant was considered total urinary fraction (T). Total fraction was then centrifuged, the new supernatant is the S1 fraction and pellet resuspended for recentrifugation, resulting in non-clustered uromodulin (S2) in the supernatant and the exosomes (Exo) in the pellet. Total urinary and S1 fractions (50ug) were precipitated by trichloroacetic acid and resuspended in loading dye. Exosomes were directly resuspended in loading dye with half the volume analyzed under the native form and the other half following deglycosylation with 750U of PNGase (New England Biolabs). Proteins were transferred on PVDF membranes that were hybridized with mouse monoclonal antibodies, 7e12 against N-terminal of polycystin-1 (51) and secondary goat anti-mouse IgG (SIGMA) coupled to horseradish peroxidase or with mouse monoclonal antibody Gapdh (Abcam, Cambridge, MA) and revealed with Amersham ECL Advance Plus (GE HealthCare) on X-Omat films.

Renal and Cardiac physiological function analysis

Renal function was evaluated by analysis of urine samples collected in metabolic cages for 24 hours with non-restricted water supply. Urinary urea nitrogen, creatinine and ion concentrations were measured with a CX9 Beckmann apparatus whereas urine osmolality was determined with a radiometer.

Proteinuria was qualitatively analyzed using 50 μg of total urinary protein on a 10 % SDS-PAGE stained with Coomassie blue as described (57).

Echocardiographic measurements on transgenic and control mice were carried out using the Vevo 770 (Visualsonics) with a probe transducer of 35MHz as in (58). Preheated ultrasound transmisson gel (Aquasonic 100) was placed on heart region to provide acoustic coupling between the probe and the mice. Cardiac dimensions including aortic root and left ventricle wall thickness and diameter were monitored in the M-mode. Functional analysis of stroke volume and cardiac output was determined from aortic Doppler measurements whereas the heart rate was obtained from ECG. Mitral and aortic valvular velocities upstream and downstream were measured using Doppler to evaluate their functional efficiency.

Morphologic, histologic, and cellular analysis

Different tissues including kidneys, heart, pancreas, lung, liver, brain, spleen were analyzed from adult transgenic mice aged between 1 to 20 months. Four-μm-thick paraffin sections of paraformaldehyde- or formalin-fixed tissues were deparaffinized and stained with hematoxylin and eosin. Detection of calcium deposits was monitored with specific stains by Alizarin red or Von Kossa and fibrosis by Sirius red.

Cysts from renal tissue were immunostained to identify the origin of the nephron segment affected. Sections (4-μm) were incubated with three primary antibodies α-calbindin (Sigma) for collecting ducts, lycopersicon esculentum lectin (Vector Lab) for distal convoluted tubules and lotus tetragonolobus lectin linked to fluorescein (Vector Lab) for proximal tubules and then with secondary antibodies a goat α-mouse IgG Alexa 255 (Invitrogen) and AMCA-streptavidin (Vector Lab). Slides were visualized with Axiovert S100TV microscope. Characterization of primary cilia in renal tissues was performed with α-

acetylated tubulin (Sigma) as primary antibody and goat α-mouse IgG Alexa 255 (Invitrogen) as secondary antibody and slides were mounted with vectashield and DAPI.

Analysis of cellular c-myc expression and proliferation using Ki67 marker was performed by immunohistochemistry (59). Kidney and liver adult mice fixed tissues from transgenic and control mice were incubated with rabbit c-myc (Upstate) or rabbit Ki67 (Novocastra) O/N at 4^0C, then for 1 hour with secondary anti-rabbit biotinylated antibody and signal detected using Vectastain ABC kit (Vector Lab) and diaminobenzinide. Proliferation rate was evaluated according to the number of renal tubules normal (control) or cystic ($Pkd1_{TAG}$) with 0, 1, ≥2 nuclei positive for Ki67 on multiple non-overlapping images (≥5) using Axiophot (Zeiss) microscope.

Vasculature analysis was performed from anesthetized animals perfused intracardiac with paraformaldehyde and Microfil media (Flow Tech Inc, Mass). Fixation was carried out overnight and tissues collected were cleared with methyl salicylate and photograph with Nikon SMZ-U using Q-capture software.

Statistical analysis

Values were expressed as mean ± standard deviation. A 2-tailed unpaired Student's t-test was used for statistical analysis; $p < 0.05$ was considered significant.

ACKNOWLEDGMENTS

We thank Dr. V. Gattone and the Indiana University School of Medicine EM Center and the generous support of that facility by the Polycystic Kidney Disease Foundation. The authors thank K. Jani for technical support and Dr C. Deschepper for critical reading of the manuscript. This work was supported by the Canadian Institutes of Health Research (CIHR) [MOP-81325 to MT] and a CIHR Frederick Banting and Charles Best studentship to AK and a Fonds de la Recherche en Santé du Québec (FRSQ) studentship to MC.

REFERENCES

1. Chapman, A.B., Rubinstein, M.D., Hughes, R., Stears, J.C., Earnest, M.P., Johnson, A.M., Gabow, P.A. and Kaehny, W.D. (1992) Intracranial aneurysms in autosomal dominant polycystic kidney disease. *N. Engl. J. of Med.,* **327,** 916-920.
2. Wei, W., Hackmann, K., Xu, H., Germino, G. and Qian, F. (2007) Characterization of cis-autoproteolysis of polycystin-1, the product of human polycystic kidney disease 1 gene. *J. Biol. Chem.,* **282,** 21729-21737.
3. Ward, C.J., Turley, H., Ong, A.C.M., Comley, M., Biddolph, S., Chetty, R., Ratcliffe, P.J., Gatter, K. and Harris, P.C. (1996) Polycystin, the polycystic kidney disease 1 protein, is expressed by epithelial cells in fetal, adult and polycystic kidney. *Proc. Natl. Acad. Sci. USA,* **93,** 1524-1528.
4. Ong, A.C.M., Ward, C.J., Butler, R.J., Biddolph, S., Bowker, C., Torra, R., Pei, Y. and Harris, P.C. (1999) Coordinate expression of the autosomal dominant polycystic kidney disease proteins, polycystin-2 and polycystin-1, in normal and cystic tissue. *Am. J. Pathol.,* **154,** 1721-1729.

5. Geng, L., Segal, Y., Peissel, B., Deng, N., Pei, Y., Carone, F., Rennke, H.G., Glücksmann-Kuis, A.M., Schneider, M.C., Ericsson, M. *et al.* (1996) Identification and localization of polycystin, the PKD1 gene product. *J. Clin. Invest.,* **98,** 2674-2682.

6. Ibraghimov-Beskrovnaya, O., Dackowski, W.R., Foggensteiner, L., Coleman, N., Thiru, S., Petry, L.R., Burn, T.C., Connors, T.D., Van Raay, T., Bradley, J. *et al.* (1997) Polycystin: In vitro synthesis, in vivo tissue expression, and subcellular localization identifies a large membrane-associated protein. *Proc. Natl. Acad. Sci. USA,* **94,** 6397-6402.

7. Chauvet, V., Qian, F., Boute, N., Cai, Y., Phakdeekitacharoen, B., Onuchic, L.F., Attie-Bitach, T., Guicharnaud, L., Devuyst, O., Germino, G.G. *et al.* (2002) Expression of *PKD1* and *PKD2* Transcripts and Proteins in Human Embryo and during Normal Kidney Development. *Am. J. Pathol.,* **160,** 973-983.

8. Peters, D.J.M., Van De Wal, A., Spruit, L., Saris, J.J., Breuning, M.H., Bruijn, J.A. and de Heer, E. (1999) Cellular Localization and Tissue Distribution of Polycystin-1. *J. Pathol.,* **188,** 439-446.

9. Trudel, M. and Guillaume, R. (2000) Molecular biology of autosomal dominant polycystic kidney disease. *Pediatr. Pathol. Mol. Med.,* **18,** 483-499.

10. Lanoix, J., D'Agati, V., Szabolcs, M. and Trudel, M. (1996) Dysregulation of cellular proliferation and apoptosis mediates human autosomal dominant polycystic kidney disease (ADPKD). *Oncogene,* **13,** 1153-1160.

11. Qian, F., Watnick, T.J., Onuchic, L.F. and Germino, G.G. (1996) The molecular basis of focal cyst formation in human autosomal dominant polycystic kidney disease type I. *Cell,* **87,** 979-987.

12. Brasier, J.L. and Henske, E.P. (1997) Loss of the polycystic kidney disease (PKD1) region of chromosome 16p13 in renal cyst cells supports a loss-of-function model for cyst pathogenesis. *J. Clin. Invest.,* **99,** 194-199.

13. Koptides, M., Constantinides, R., Kyriakides, G., Hadjigavriel, M., Patsalis, P.C., Pierides, A. and Deltas, C.C. (1998) Loss of heterozygosity in polycystic kidney disease with a missense mutation in the repeated region of PKD1. *Hum. Genet.,* **103,** 709-717.

14. Guillaume, R., D'Agati, V., Daoust, M. and Trudel, M. (1999) Murine Pkd1 is a developmentally regulated gene from morula to adulthood: Role in tissue condensation and patterning. *Dev. Dyn.,* **214,** 337-348.

15. Guillaume, R. and Trudel, M. (2000) Distinct and common developmental expression patterns of the murine PKD2 and PKD1 genes. *Mech. Dev.,* **93,** 179-183.

16. Boulter, C., Mulroy, S., Webb, S., Fleming, S., Brindle, K. and Sandford, R. (2001) Cardiovascular, skeletal, and renal defects in mice with a targeted disruption of the *Pkd1* gene. *Proc. Natl. Acad. Sci. USA,* **98,** 12174-12179.

17. Kim, K., Drummond, I., Ibraghimov-Beskrovnaya, O., Klinger, K. and Arnaout, M.A. (2000) Polycystin 1 is required for the structural integrity of blood vessels. *Proc. Natl. Acad. Sci. USA,* **97,** 1731-1736.

18. Lu, W., Peissel, B., Babakhanlou, H., Pavlova, A., Geng, L., Fan, X., Larson, C., Brent, G. and Zhou, J. (1997) Perinatal lethality with kidney and pancreas defects in mice with a targetted PKD1 mutation. *Nat. Genet.,* **17,** 179-181.

19. Lu, W., Shen, X., Pavlova, A., Lakkis, M., Watrd, C.J., Pritchard, L., Harris, P.C., Genest, D.R., Perez-Atayde, A.R. and Zhou, J. (2001) Comparison of *Pkd1*-targeted mutants reveals that loss of polycystin-1 causes cystogenesis and bone defects. *Hum. Mol. Genet.,* **10,** 2385-2396.

20. Muto, S., Aiba, A., Saito, Y., Nakao, K., Nakamura, K., Tomita, K., Kitamura, T., Kurabayashi, M., Nagai, R., Higashihara, E. *et al.* (2002) Pioglitazone improves the phenotype and molecular defects of a targeted *Pkd1* mutant. *Hum. Mol. Genet.,* **11,** 1731-1742.

21. Wu, G., Tian, X., Nishimura, S., Markowitz, G.S., D'Agati, V., Park, J.H., Yao, L., Li, L., Geng, L., Zhao, H. *et al.* (2002) *Trans*-heterozygous *Pkd1* and *Pkd2* mutations modify expression of polycystin kidney disease. *Hum. Mol. Genet.,* **11,** 1845-1854.

22. Starremans, P.G., Li, X., Finnerty, P.E., Guo, L., Takakura, A., Neilson, E.G. and Zhou, J. (2008) A mouse model for polycystic kidney disease through a somatic in-frame deletion in the 5' end of Pkd1. *Kidney Int.,* **73,** 1394-1405.

23. Lantinga-van Leeuwen, I.S., Leonhard, W.N., van der Wal, A., Breuning, M.H., de Heer, E. and Peters, D.J.M. (2007) Kidney-specific inactivation of the Pkd1 gene induces rapid cyst formation in developing kidneys and a slow onset of disease in adult mice. *Hum. Mol. Genet.,* **16,** 3188-3196.

24. Takakura, A., Contrino, L., Beck, A.W. and Zhou, J. (2008) Pkd1 inactivation induced in adulthood produces focal cystic disease. *J. Am. Soc. Nephrol.,* **19,** 2351-2363.

25. Lantinga-van Leeuwen, I.S., Dauwerse, J.G., Baelde, H.J., Leonhard, W.N., van de Wal, A., Ward, C.J., Verbeek, S., Deruiter, M.C., Breuning, M.H., de Heer, E. *et al.* (2004) Lowering of *Pkd1* expression is sufficient to cause polycystic kidney disease. *Hum. Mol. Genet.,* **13,** 3069-3077.

26. Lu, W., Fan, X., Basora, N., Babakhanlou, H., Law, T., Rifai, N., Harris, P.C., Perez-Atayde, A.R., Rennke, H.G. and Zhou, J. (1999) Late onset of renal and hepatic cysts in *Pkd1*-targeted heterozygotes. *Nat. Genet.,* **21,** 160-161.

27. Thivierge, C., Kurbegovic, A., Couillard, M., Guillaume, R., Cote, O. and Trudel, M. (2006) Overexpression of PKD1 Causes Polycystic Kidney Disease. *Mol. Cell. Biol.,* **26,** 1538-1548.

28. Trudel, M., D'Agati, V. and Costantini, F. (1991) C-myc as an inducer of polycystic kidney disease in transgenic mice. *Kidney Int.,* **39,** 665-671.

29. Torres, V.E., Erickson, S.B., Smith, L.H., Wilson, D.M., Hattery, R.R. and Segura, J.W. (1988) The association of nephrolithiasis and autosomal dominant polycystic kidney disease. *Am. J. Kidney Dis.,* **11,** 318-325.

30. Torres, V.E., Wilson, D.M., Hattery, R.R. and Segura, J.W. (1993) Renal stone disease in autosomal dominant polycystic kidney disease. *Am. J. Kidney Dis.,* **22,** 513-519.

31. Levine, E. and Grantham, J.J. (1992) Calcified renal stones and cyst calcifications in autosomal dominant polycystic kidney disease: clinical and CT study in 84 patients. *Am. J. Roentgenol.,* **159,** 77-81.

32. Gonzales, P.A., Pisitkun, T., Hoffert, J.D., Tchapyjnikov, D., Star, R.A., Kleta, R., Wang, N.S. and Knepper, M.A. (2009) Large-scale proteomics and phosphoproteomics of urinary exosomes. *J. Am. Soc. Nephrol.,* **20,** 363-379.

33. Hogan, M.C., Manganelli, L., Woollard, J.R., Masyuk, A.I., Masyuk, T.V., Tammachote, R., Huang, B.Q., Leontovich, A.A., Beito, T.G., Madden, B.J. *et al.* (2009) Characterization of PKD protein-positive exosome-like vesicles. *J. Am. Soc. Nephrol.,* **20,** 278-288.

34. Adeney, K.L., Siscovick, D.S., Ix, J.H., Seliger, S.L., Shlipak, M.G., Jenny, N.S. and Kestenbaum, B.R. (2009) Association of serum phosphate with vascular and valvular calcification in moderate CKD. *J. Am. Soc. Nephrol.,* **20,** 381-387.

35. Yoder, B.K., Hou, X. and Guay-Woodford, L.M. (2002) The Polycystic Kidney Disease Proteins, Polycystin-1, Polycystin-2, Polaris, and Cystin, Are Co-Localized in Renal Cilia. *J. Am. Soc. Nephrol.,* **13,** 2508-2516.

36. Pazour, G.J., Dickert, B.L., Vucica, Y., Seeley, E.S., Rosenbaum, J.L., Witman, G.B. and Cole, D.G. (2000) Chlamydomonas IFT88 and its mouse homologue, polycystic kidney disease gene tg737, are required for assembly of cilia and flagella. *J. Cell. Biol.,* **151,** 709-718.

37. Lin, F., Hiesberger, T., Cordes, K., Sinclair, A.M., Goldstein, L.S.B., Somlo, S. and Igarashi, P. (2003) Kidney-specific inactivation of the KIF3A subunit of kinesin-II inhibits renal ciliogenesis and produces polycystic kidney disease. *Proc. Natl. Acad. Sci. USA,* **100,** 5286-5291.

38. Masyuk, T.V., Huang, B.Q., Ward, C.J., Masyuk, A.I., Yuan, D., Splinter, P.L., Punyashthiti, R., Ritman, E.L., Torres, V.E., Harris, P.C. *et al.* (2003) Defects in cholangiocyte fibrocystin expression and ciliary structure in the PCK rat. *Gastroenterology,* **125,** 1303-1310.

39. Smith, L.A., Bukanov, N.O., Husson, H., Russo, R.J., Barry, T.C., Taylor, A.L., Beier, D.R. and Ibraghimov-Beskrovnaya, O. (2006) Development of polycystic kidney disease in juvenile cystic kidney mice: insights into pathogenesis, ciliary abnormalities, and common features with human disease. *J. Am. Soc. Nephrol.,* **17,** 2821-2831.

40. Cadieux, C., Harada, R., Paquet, M., Cote, O., Trudel, M., Nepveu, A. and Bouchard, M. (2008) Polycystic kidneys caused by sustained expression of Cux1 isoform p75. *J. Biol. Chem.,* **283,** 13817-13824.

41. Pisitkun, T., Shen, R.F. and Knepper, M.A. (2004) Identification and proteomic profiling of exosomes in human urine. *Proc. Natl. Acad. Sci. U S A,* **101,** 13368-13373.

42. Jiang, S.-T., Chiou, Y.-Y., Wang, E., Lin, H.-K., Lin, Y.-T., Chi, Y.-C., Wang, C.-K.L., Tang, M.-J. and Li, H. (2006) Defining a Link with Autosomal-Dominant Polycystic Kidney Disease in Mice with Congenitally Low Expression of Pkd1. *Am. J. Pathol.,* **168,** 205-220.

43. Trudel, M. and D'Agati, V. (1992) A model of polycystic kidney disease in SBM transgenic mice. In Berlyne, G.M. (ed.), *Contrib. Nephrol.* Karger, S., Basel, Brooklyn, NY, Vol. 97, pp. 47-59.

44. Griffin, M.D., Torres, V.E., Grande, J.P. and Kumar, R. (1996) Immunolocalization of polycystin in human tissues and cultured cells. *Proc. Assoc. Am. Physicians,* **108**.

45. Leier, C.V., Baker, P.B., Kilman, J.W. and Wooley, C.F. (1984) Cardiovascular abnormalities associated with adult polycystic kidney disease. *Ann. Intern. Med.,* **100,** 683-688.

46. Hossack, K.F., Leddy, C.L., Johnson, A.M., Schrier, R.W. and Gabow, P.A. (1988) Echocardiographic findings in autosomal dominant polycystic kidney disease. *The New England Journal of Medicine,* **319,** 907-912.

47. Griffin, M.D., Torres, V.E., Grande, J.P. and Kumar, R. (1997) Vascular Expression of Polycystin. *J. Am. Soc. Nephrol.,* **8,** 616-626.

48. Peters, D.J.M., Spruit, L., Klingel, R., Prins, F., Baelde, H.J.J., Giordano, P.C., Bernini, L.F., de Heer, E., Breuning, M.H. and Bruijn, J.A. (1996) Adult, fetal, and polycystic kidney expression of polycystin, the polycystic kidney disease-1 gene product. *Lab. Invest.,* **75,** 221-230.

49. Weston, B.S., Jeffery, S., Jeffrey, I., Sharaf, S.F.A., Carter, N., Saggar-Malik, A. and Price, R.G. (1997) Polycystin expression during embryonic development of human kidney in adult tissues and ADPKD tissue. *Histochem. J.,* **29,** 847-856.

50. Palson, R., Sharma, C.P., Kim, K., McLaughlin, M., Brown, D. and Arnaout, M.A. (1996) Characterization and cell distribution of polycystin, the product of autosomal dominant polycystic kidney disease gene 1. *Mol. Med.,* **2,** 702-711.

51. Ong, A.C.M., Harris, P.C., Davies, D.R., Pritchard, L., Rossetti, S., Biddolph, S., Vaux, D.J.T., Migone, N. and Ward, C.J. (1999) Polycystin-1 expression in PKD1, early onset PKD1 and TSC2/PKD1 cystic tissue: implications for understanding cystogenesis. *Kidney Int.,* **56,** 1324-1333.

52. Pritchard, L., Sloane-Stanley, J.A., Sharpe, J.A., Aspinwall, R., Lu, W., Buckle, V., Strmecki, L., Walker, D., Ward, C.J., Alpers, C.E. *et al.* (2000) A human *PKD1* transgene generates functional polycystin-1 in mice and is associated with a cystic phenotype. *Hum. Mol. Genet.,* **9,** 2617-2627.

53. Ahrabi, A.K., Terryn, S., Valenti, G., Caron, N., Serradeil-Le Gal, C., Raufaste, D., Nielsen, S., Horie, S., Verbavatz, J.M. and Devuyst, O. (2007) PKD1 haploinsufficiency causes a syndrome of inappropriate antidiuresis in mice. *J. Am. Soc. Nephrol.,* **18,** 1740-1753.

54. Gong, S., Yang, X.W., Li, C. and Heintz, N. (2002) Highly Efficient Modification of Bacterial Artificial Chromosomes (BACs) Using Novel Shuttle Vectors Containing the R6Kγ Origin of Replication. *Genome Res.,* **12,** 1992-1998.

55. Couillard, M., Guillaume, R., Tanji, N., D'Agati, V. and Trudel, M. (2002) c-myc-induced Apoptosis in Polycystic Kidney Disease is Independent of FasL/Fas Interaction. *Cancer Res.,* **62,** 2210-2214.

56. Trudel, M., Lanoix, J., Barisoni, L., Blouin, M.-J., Desforges, M., L'Italien, C. and D'Agati, V. (1997) C-myc-induced Apoptosis in Polycystic Kidney Disease is Bcl-2 and p53 Independent. *J. Exp. Med.,* **186,** 1873-1884.

57. De Paepe, M.E. and Trudel, M. (1994) The transgenic SAD mouse: A model of human sickle cell glomerulopathy. *Kidney Int.,* **46,** 1337-1345.

58. Stoyanova, E., Trudel, M., Felfly, H., Garcia, D. and Cloutier, G. (2007) Characterization of circulatory disorders in beta-thalassemic mice by noninvasive ultrasound biomicroscopy. *Physiol. Genomics,* **29,** 84-90.

59. Couillard, M. and Trudel, M. (2009) C-myc as a modulator of renal stem/progenitor cell population. *Dev. Dyn.,* **238,** 405-414.

FIGURE LEGENDS

Figure 1 Genomic analysis of Pkd1 $_{TAG}$ transgenic mice

Representative analysis of the 5' regulatory region of Pkd1$_{TAG}$ transgenic mice was carried out based on a polymorphism at ~ 4.5 kb upstream of the translation initiation codon of the murine *Pkd1* gene. Since Pkd1$_{TAG}$ transgenic mice were produced on a mixed C57Bl6/J and CBA/J inbred background, the BAC of 129sv origin could be detected by 100bp amplification band whereas the C57Bl6/J and CBA/J displayed a 133 and 113bp, respectively. Analysis of the 3' Pkd1$_{TAG}$ region was verified on Southern using a KpnI digestion with the Pkd1 "g" probe (exon 45-46). Bands are expected at 7kb for the endogenous Pkd1 gene and at 5kb for the Pkd1$_{TAG}$ transgene (5kb). The 5' and the 3' ends of the transgene were intact for the three transgenic mouse lines. M: 100 bp marker; C: negative control; C57: C57Bl/6J mice; CBA: CBA/J mice; 129:129sv mice; Ma: lambda HindIII marker; WT: wild type control mice; Tg: Pkd1$_{TAG}$ transgene; Endo: endogenous Pkd1 gene; E: EcoRI; K: Kpnl; E* = tag silent point mutation.

Figure 2 Expression analysis of Pkd1 $_{TAG}$ transgenic mice

(**A**) Renal expression analysis of total *Pkd1* (endogenous and transgene: ~14.2kb) transcript of Pkd1$_{TAG}$ transgenic mice assessed by Northern blotting using Pkd1 probe "f" (exon 36-45) and Gapdh (1.2 kb). One representative kidney sample from each transgenic line 6, 18 and 26 is compared to endogenous *Pkd1* transcript of control (C) genetic background and age-matched mice. Quantification of renal transcripts from transgenic Pkd1$_{TAG}$ mouse lines were increased compared to endogenous Pkd1 transcript as indicated below the blot (control refers to 1).

(**B**) Quantitative real-time PCR of Pkd1 expression from renal and extrarenal tissues was carried out using primers in exons 1 and 2. Transgenic mice (n=3; * n= 2) from each of the 3 different lines and non-transgenic age-matched control mice (4-12 mo) were analyzed in triplicata for Pkd1 and S16 that served as an internal control. Quantification of renal expression in these transgenic mice ranged from 1.3

to 15.5-fold relative to endogenous levels of control mice arbitrarily set at 1. Extrarenal tissue expression levels were established in function of Pkd1 levels in control kidneys. Number in parentheses refers to the ratio of transgene expression levels to the organ control. Similar gene expression ratio or fold-increase was detected for each transgenic line across the tissues analyzed.

(**C**) Renal and extrarenal polycystin-1 protein expression analysis in $Pkd1_{TAG}$ 26 mice (6 mo.) by Western blot using the N-terminal Pc-1 7e12antibody. In $Pkd1_{TAG}$ organs, Pc-1 expression was intact and at higher expression levels than controls (6 mo.). Of the organs tested, highest Pc-1 signal was detected in lungs, heart and kidney. Quantities of protein loaded (40 or 80 ug prot) are indicated below the blot. C: non-transgenic control mice; Tg: $Pkd1_{TAG}$ transgenic mice, line 26. Gapdh was used as an internal loading control.

Figure 3 Renal phenotype in $Pkd1_{TAG}$ mice

(**A, B**) Overview of renal cortical sections from adult 20 month-old control and $Pkd1_{TAG}6$ mice, respectively. While control exhibited normal glomeruli (g) and tubule (t), $Pkd1_{TAG}6$ mice showed presence of numerous glomerular and tubular cysts associated with frequent proteinaceous casts (pc) and of tubulointerstitial fibrosis (H&E). Original magnification, x10.

(**C, D**) High power view of renal sections of $Pkd1_{TAG}6$ and 26 mice (26 and 16 mo.) that show epithelial hyperplasia and hypertrophy (H) as well as presence of polyps (arrowhead) in cystic tubules. Original magnification, x 40.

(**E, F**) Assessment of nephron segment origin in control and $Pkd1_{TAG}26$ mice (7 mo.) respectively was determined by immunofluorescence using specific markers of proximal (Lotus tetragonolobus, green), distal (Esculentum Lycopersicon, blue) and collecting ducts (α-Calbindin D28K, red). Transgenic mice displayed cysts from all nephron segments and in higher proportion in proximal and collecting tubules. Noticeably, epithelial hyperplasia and hypertrophy (H) were frequently observed in dilated collecting ducts. Original magnification, x20.

(**G, H**) Analysis of calcium deposits from renal sections of control and $Pkd1_{TAG}26$ (10 mo.) respectively was evaluated by Alizarin red staining. Intense extracellular calcium deposits were detected in the renal papilla of $Pkd1_{TAG}26$ mice (inset) but absence of signal in cysts or in kidneys of non-transgenic mice. Original magnification, x10.

(**I, J**) Proliferation was assessed from control and $Pkd1_{TAG}26$ renal sections (13 mo.) respectively with the Ki67 nuclear proliferation marker. Epithelial cells from normal and dilated tubules displayed higher rate of proliferation in $Pkd1_{TAG}26$ mice compared to control. Original magnification, x40.

(**K, L**) Detection of c-myc in renal tissues of control and $Pkd1_{TAG}6$ (13 mo.) respectively correlated with higher proliferation rate. Increased nuclear and even cytoplasmic staining in cystic and non-cystic regions in $Pkd1_{TAG}6$ relative to control. Original magnification, x40.

(**M, N**) Primary cilia of renal epithelial cells from control and $Pkd1_{TAG}$ mice (1 mo.) respectively were assessed. Triplet figure consists of staining by α-acetylated tubulin (left panel) marker for cilia, DAPI (middle panel) for nucleus and merge (right panel). In control mice, the average length of cilia was estimated to 2-3 μm whereas in $Pkd1_{TAG}26$ mice a significant shift in cilia length distribution to longer cilia of ≥ 5 μm was measured. Original magnification, x100.

Figure 4 Analysis of urinary proteins in $Pkd1_{TAG}$ mice

(**A**) Protein urine samples from all $Pkd1_{TAG}$ mice lines (4 mo.) were compared to non-transgenic age-matched control (C) and SBM transgenic mice (positive control that develop PKD) in addition to serum protein sample (S) from non-transgenic mice on SDS-PAGE stained by Coomassie blue. Albumin normally present in serum was detected at abnormally high levels in $Pkd1_{TAG}26$ urine comparable to SBM urine. $Pkd1_{TAG}$ mice like SBM mice exhibit non-selective proteinuria. Mice also displayed normal excretion of the major urinary proteins (MUPs). M: molecular mass markers of 31 to 200 kDa.

(**B**) Polycystin-1 was analyzed in fractioned urinary samples by Western blot using the N-terminal 7e12 Pc-1 antibody. Two bands (slightly above ~420kDa and ~360-380kDa) were typically detected in native

(N, without treatment) samples whether from total kidney protein extracts of $Pkd1_{TAG}26$, from total urinary proteins (T) or exosome-free fraction (S1) of $Pkd1_{TAG}26$ and of control mice (mean ~9 mo.). A unique Pc-1 band slightly above ~420kDa was observed in exosome (Exo) fractions from $Pkd1_{TAG}$ and control urine whereas the uromodulin-positive (S2) fraction appears devoided of Pc-1. Noticeably, $Pkd1_{TAG}$ transgenic mice in comparison to age-matched control mice consistently showed more intense Pc-1 bands and likely higher Pc-1 excretion. Upon deglycosylation (DG) of protein extracts with PNGase, a unique band is detected at the size of the lowest native band (~360-380kDa), showing strong glycosylation of Pc-1 and indicating that the band above ~420kDa is likely the cleaved form of Pc-1 (predicted mass of 448kDa and 328kDa in glycosylated and deglycosylated respectively).

Figure 5 $Pkd1_{TAG}$ mice hepatic phenotypes

(**A, B**) Macroscopic view of livers is shown from adult control and $Pkd1_{TAG}$ 26 mice (20 mo.) respectively. In comparison to normal liver of control mice, liver of $Pkd1_{TAG}$ mice appeared abnormal with clusters of cysts. Original magnification, x5.

(**C, D**) Overview of liver histologic sections from adult control and $Pkd1_{TAG}26$ mice (14 and 23 mo.), respectively. Notably, a $Pkd1_{TAG}$ mouse shows presence of numerous cysts (c) lined by cuboid epithelium, suggesting tubular cholangiocyte origin. Cluster of cysts are formed focally around the periportal region tubular structures (H&E). Original magnification, x10.

(**E, F**) Liver sections from adult control and $Pkd1_{TAG}26$ mice (11and 14 mo.), respectively. Liver of $Pkd1_{TAG}$ mice displayed severe periportal fibrosis with various levels of increased interstitial fibrosis (Sirius red). Original magnification, x10.

(**G, H**) Proliferation was assessed from liver sections of control and $Pkd1_{TAG}26$ (21 mo.) respectively with the Ki67 nuclear proliferation marker. Cystic epithelium of the liver was associated with higher rate of proliferation compared to non-cystic control. Original magnification, x40.

(**I, J**) Analysis of c-myc in hepatic tissues of control and $Pkd1_{TAG}26$ (16 and 23 mo.) respectively correlated with higher proliferation rate. Increased nuclear and even cytoplasmic staining is observed in cystic regions in $Pkd1_{TAG}$ relative to control. Original magnification, x40.

Figure 6 Cardiac phenotypes in $Pkd1_{TAG}$ mice

(**A, B**) Non-invasive ultrasound of cardiac function of adult control mice and $Pkd1_{TAG}$ 26 mice (16 mo.), respectively. Echocardiography of $Pkd1_{TAG}$ mice detected presence of aortic valve of hyperechoic, indicating calcification and probably stenosis (white arrow). Attached video imaging shows the inability of the aortic valves to fully open.

(**C, D**) Anatomy of hearts from adult control mice and $Pkd1_{TAG}$ mice (8 and 7 mo.), respectively. The heart size of $Pkd1_{TAG}$ mice (0.32g and body weight 16.7g) is readily larger than non-transgenic control (0.27g and body weight 31.5g). Original magnification, x2.5.

(**E, F**) Heart vasculature from adult control mice and $Pkd1_{TAG}$ 26 mice (11 and 13 mo.) respectively, filled with Microfil latex. $Pkd1_{TAG}$ mouse left ventricle hypertrophy was clearly visible under 3D angles by different segmentation and the substantial decreased vascularization of ventricular wall (*).

(**G, H**) Longitudinally sectioned heart from adult control and $Pkd1_{TAG}$ mice (11 and 12 mo.), respectively. View of sectioned heart of $Pkd1_{TAG}$ 26 mouse displays changes in color pigmentation of the left ventricle wall (arrow) due to calcium deposits as defined with specific histology stains. Original magnification, x5.

(**I, J**) Higher-power view of aortic valves from adult control and $Pkd1_{TAG}$ mice (11 and 12 mo.), respectively. $Pkd1_{TAG}$ mouse exhibited severe calcified valves (arrow) stained with Alizarin red consistent with echocardiography. Original magnification, x20.

Figure 7 $Pkd1_{TAG}$ mice vascular defect: intracranial aneurysm.

(**A, B**) Macroscopic view of scalped head is shown from adult control and $Pkd1_{TAG}$26 mice (1 mo.) respectively. Evidence of enlarged skull associated with abnormal brain/ventricle morphology, sagital suture, intracranial hemorrhages and edema in $Pkd1_{TAG}$ mice.

(**C, D**) Overview of brain sections from adult control and $Pkd1_{TAG}$ mice (1 mo.), respectively. Evidence of $Pkd1_{TAG}$ cortex (c) thinning is shown with a major cavity associated with elongated and compressed cerebellum (ce) due to hemorrhage and excessive fluid (H&E). Original magnification, x1.25.

(**E, F**) Brain vasculature from adult control mice and $Pkd1_{TAG}$ 26 mice (11 and 13 mo.) respectively filled with Microfil latex. Evidence of unruptured cerebral aneurysm (arrow) was observed in a $Pkd1_{TAG}$ mouse whereas not detected in vasculature of control mice. Original magnification, x5.

Table 1

A) Urine Analysis

Mice*	Age (mo)	n	Volume (mL)	n	Urea Nitrogen (mmol/L)	n	Creatinine (mmol/L)	n	Protein (g/L)	n	Osmolality (mOsm/kg)
Control	16	5	**0.5** ± 0.2	5	**682** ± 407	5	**4.9** ± 0.6	5	**1.4** ± 0.8	5	**2026** ± 160
$Pkd1_{TAG}$ 6	15	6	**1.6** ± 0.5[b]	6	**309** ± 148 [c]	6	**1.1** ± 0.3[d]	6	**0.7** ± 0.3	6	**627** ± 166[d]
Control	4-9	12	**0.7** ± 0.4	12	**809** ± 320	15	**3.9** ± 1.8	11	**6.9** ± 5.5	11	**1426** ± 547
SBM	4-10	10	**2.7** ± 1.3[b]	7	**328** ± 76[c]	8	**1.3** ± 0.6[c]	5	**3.4** ± 1.4	4	**843** ± 265[a]
$Pkd1_{TAG}$ 26	5-7	7	**2.4** ± 1.5[b]	8	**461** ± 267[a]	10	**1.6** ± 1.3[b]	8	**1.1** ± 0.7[b]	6	**985** ± 566

*Urine analysis of $Pkd1_{TAG}$ with control mice at severe renal phenotype time points.
[a] P≤0.02; [b] P≤0.01; [c] P≤0.001; [d] P≤0.0001

B) Blood Analysis

Mice	Age (mo)	n	Hematocrit (%)	n	BUN range (mmol/L)	Creatinine (mmol/L)	Sodium (mmol/L)	Osmolality (mOsm/kg)
Control	6	5	**54** ± 3	5	**6.3 – 8.4** (mean 7.5 ± 0.8)	**19.6** ± 2.6	**151** ± 2	**329** ± 5
$Pkd1_{TAG}$ 6	15	6	**40** ± 3[e]	6	**9.0 – 12.8**	**20.1** ± 3.2	**157** ± 2[d]	**340** ± 4[b]
$Pkd1_{TAG}$ 26	6	7	**35** ± 6[c]	8	**5.5 – 10.8**	**29.8** ± 7.5[b]	**156** ± 2[b]	**336** ± 6[a]

[a] P≤0.05; [b] P≤0.005; [c] P≤0.001; [d] P≤0.0005; [e] P≤0.0001

Table 2

A) Cardiac Dimension Analysis

Mice		Heart wt/ Body wt		Echocardiographic measurement: Left ventricle pw		Inter-ventricular septum		Aortic root		Left ventricle volume		Ventricle diameter	
				d	s	d	s	diam.	area	d	s	d	s
		%		10^{-2} mm/wt		10^{-2} mm/wt		10^{-2} mm/wt		µl/wt		10^{-2} mm/wt	
	n		n										
Control	21	**0.7** ±0.1	6	**2.0** ±0.3	**2.8** ±0.6	**2.1** ±0.4	**3.0** ±0.5	**3.5** ±0.2	**4.1** ±0.3	**2.21** ±0.23	**1.01** ±0.24	**10.7** ±0.7	**7.7** ±0.9
$Pkd1_{TAG}6$	26	**0.9**[a] ±0.3	6	**3.8**[c] ±0.6	**5.1**[d] ±0.7	**3.6**[d] ±0.4	**4.9**[d] ±0.5	**5.0**[b] ±0.8	**5.3**[a] ±1.0	**2.17** ±0.35	**0.73** ±0.23	**13.9**[c] ±1.2	**8.8** ±1.1
$Pkd1_{TAG}26$	27	**1.0**[e] ±0.2	4	**3.3**[c] ±0.4	**4.6**[b] ±0.6	**3.2**[a] ±0.6	**4.0** ±1.3	**5.0**[d] ±0.2	**5.7**[d] ±0.2	**3.11** ±1.06	**1.51** ±0.97	**15.2**[a] ±2.4	**10.9** ±3.0

[a] P≤0.05; [b] P≤0.003; [c] P≤0.002; [d] P≤0.0002; [e] P≤10^{-6}
wt = weight; pw = posterior wall; d = diastolic; s = systolic; diam. = diameter

B) Echocardiographic Functional Analysis

Mice		Stroke vol. aorta	Fractional ejection	Fractional shortening	Cardiac output	Heart rate		Aortic valve velocity: Upstream mean	Aortic valve velocity: Upstream peak		Aortic valve velocity: Downstream mean	Aortic valve velocity: Downstream peak		Mitral valve velocity: Upstream mean	Mitral valve velocity: Upstream peak		Mitral valve velocity: Downstream mean	Mitral valve velocity: Downstream peak
		10^{-2} mL/wt	%	%	ml/min/wt	bpm		mm/s			mm/s			mm/s			mm/s	
	n						n			n			n			n		
Control	6	**0.27** ±0.03	**54.8** ±6.5	**28.5** ±4.3	**1.29** ±0.16	**474** ±16	4	**554** ±56	**977** ±140	6	**1152** ±134	**1901** ±247	4	**557** ±79	**899** ±105	6	**743** ±77	**1247** ±133
$Pkd1_{TAG}6$	6	**0.31** ±0.06	**66.6**[b] ±8.1	**36.4**[b] ±6.2	**1.49** ±0.32	**482** ±22	6	**486** ±104	**776** ±170	6	**1155** ±343	**1861** ±565	6	**511** ±74	**851** ±135	6	**800** ±117	**1318** ±208
$Pkd1_{TAG}26$	4	**0.53**[b] ±0.13	**53.6** ±17.1	**28.5** ±12.2	**2.59**[c] ±0.46	**487** ±43	4	**581** ±251	**965** ±431	4	**1705**[a] ±344	**2772**[a] ±562	4	**454** ±103	**817** ±156	4	**714** ±109	**1233** ±205

[a] P≤0.05; [b] P≤0.03; [c] P≤0.01
bpm = beats per minute

Figure 1

5' analysis:

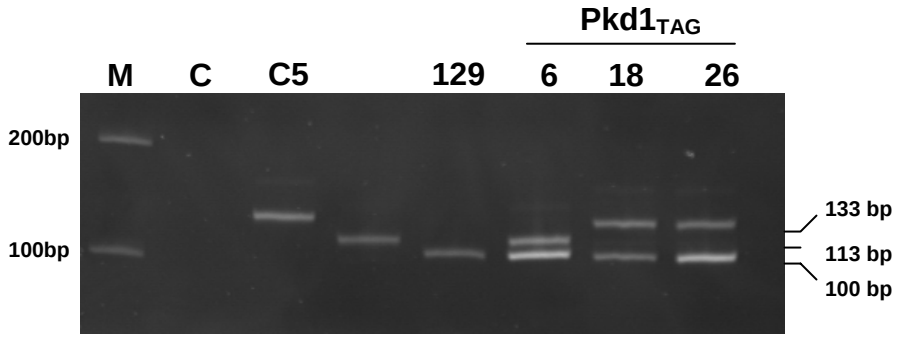

3' analysis: Pkd1 Probe/KpnI

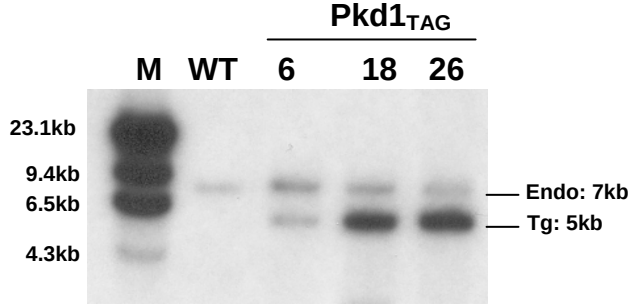

Figure 2

A

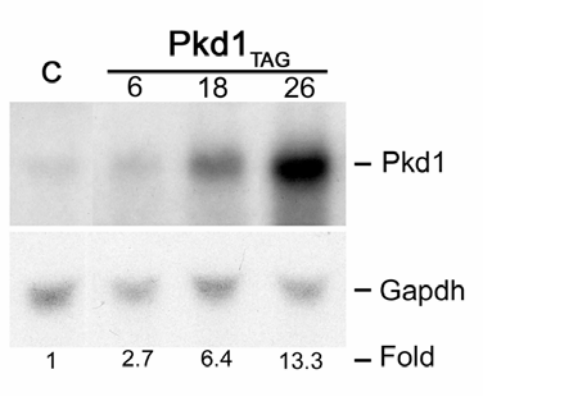

B

Mice	n	Pkd1 expression relative to control kidneys (relative to organ control)						
		Kidneys	Brain	Heart	Lungs	Spleen	Liver	Pancreas
Control	3	1.0	3.5 (1.0)	1.5 (1.0)	2.9 (1.0)	0.5 (1.0)	0.6 (1.0)	0.8 (1.0)
$Pkd1_{TAG}$ 6	3	1.3	5.6 (1.6)	2.3 (1.5)	3.1 (1.1)	0.7 (1.4)	0.8 (1.2)	1.0 (1.2)
$Pkd1_{TAG}$ 18	3	8.0	24.7 (7.1)	13.6 (8.8)	13.9 (4.9)	3.5 (6.6)	3.2 (5.3)	3.0 (3.6)
$Pkd1_{TAG}$ 26	3	15.5	37.7 (10.8)	20.6 (13.3)	22.6 (7.9)	5.8 (11.0)	5.3 (8.7)	10.9 (13.2) *

C

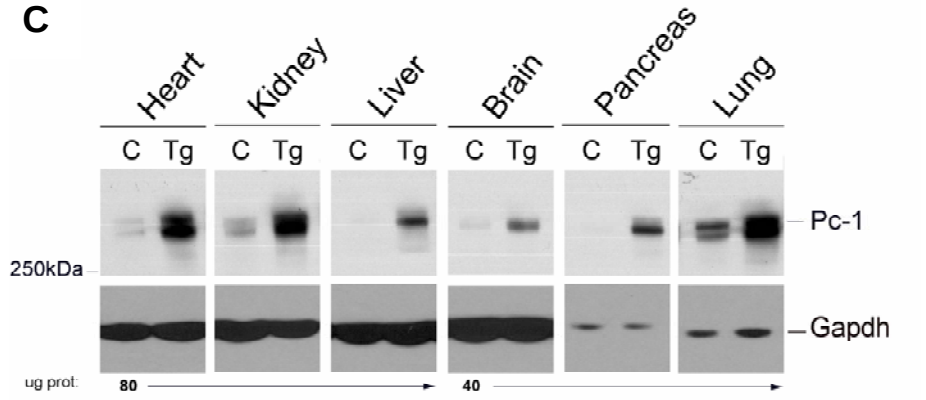

Figure 3

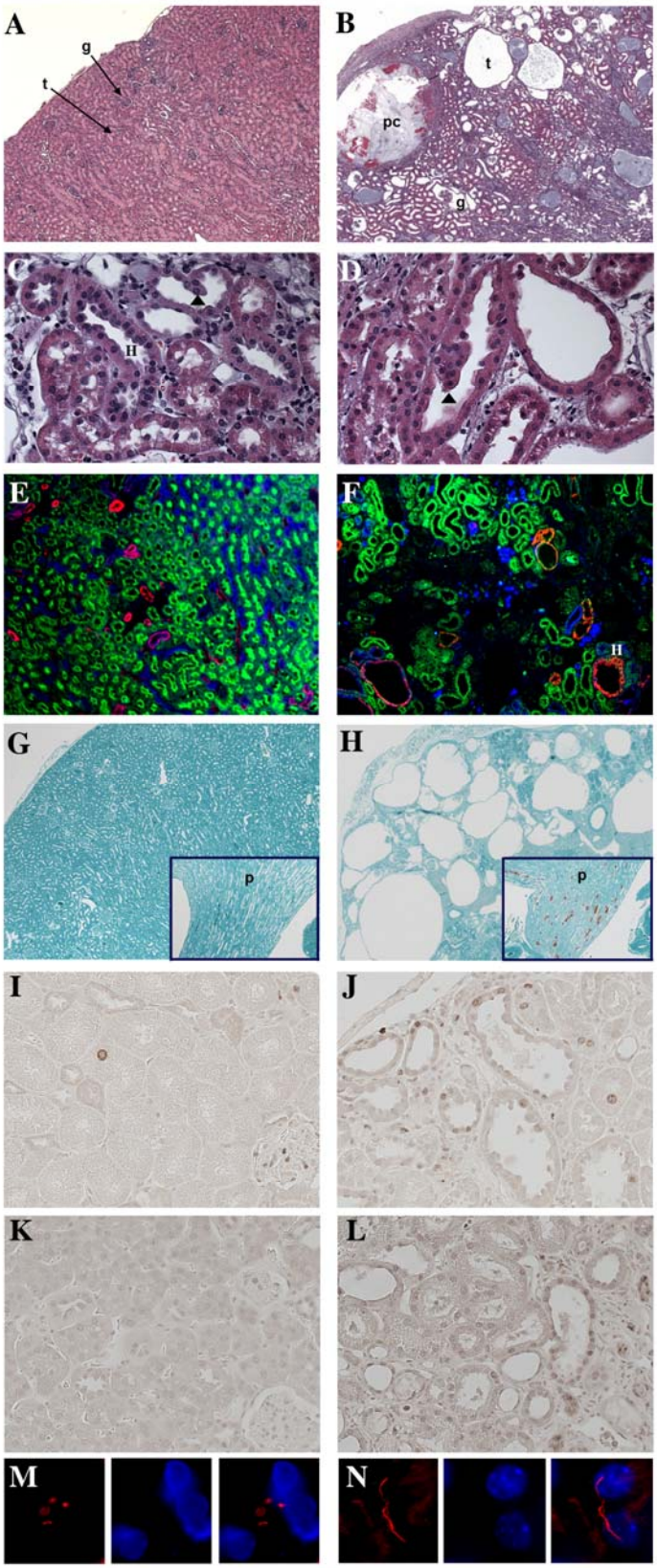

Figure 4

A

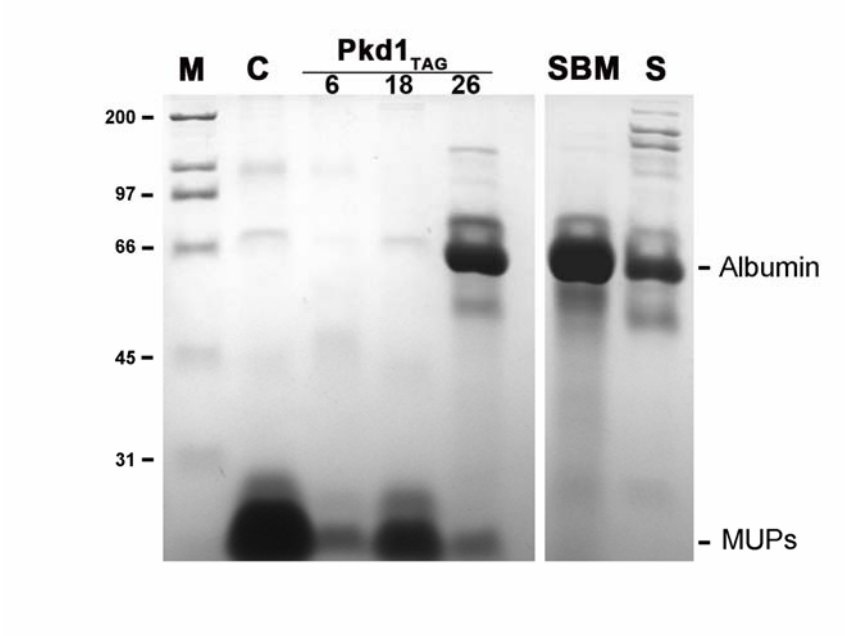
M
C
Pkd1TAG
6
18
26
SBM
S
200
97
66
45
31
Albumin
MUPs

B

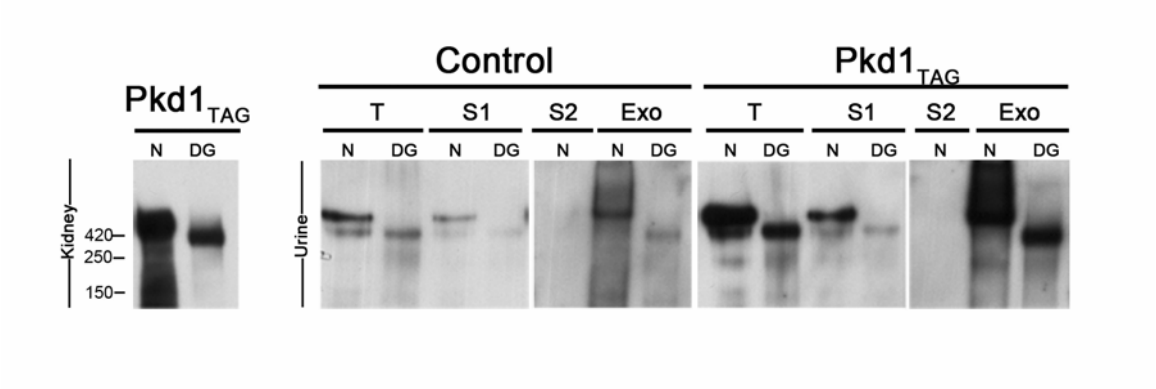
Pkd1TAG
N
DG
Kidney
420
250
150
Control
Pkd1TAG
T
S1
S2
Exo
Urine

Figure 5

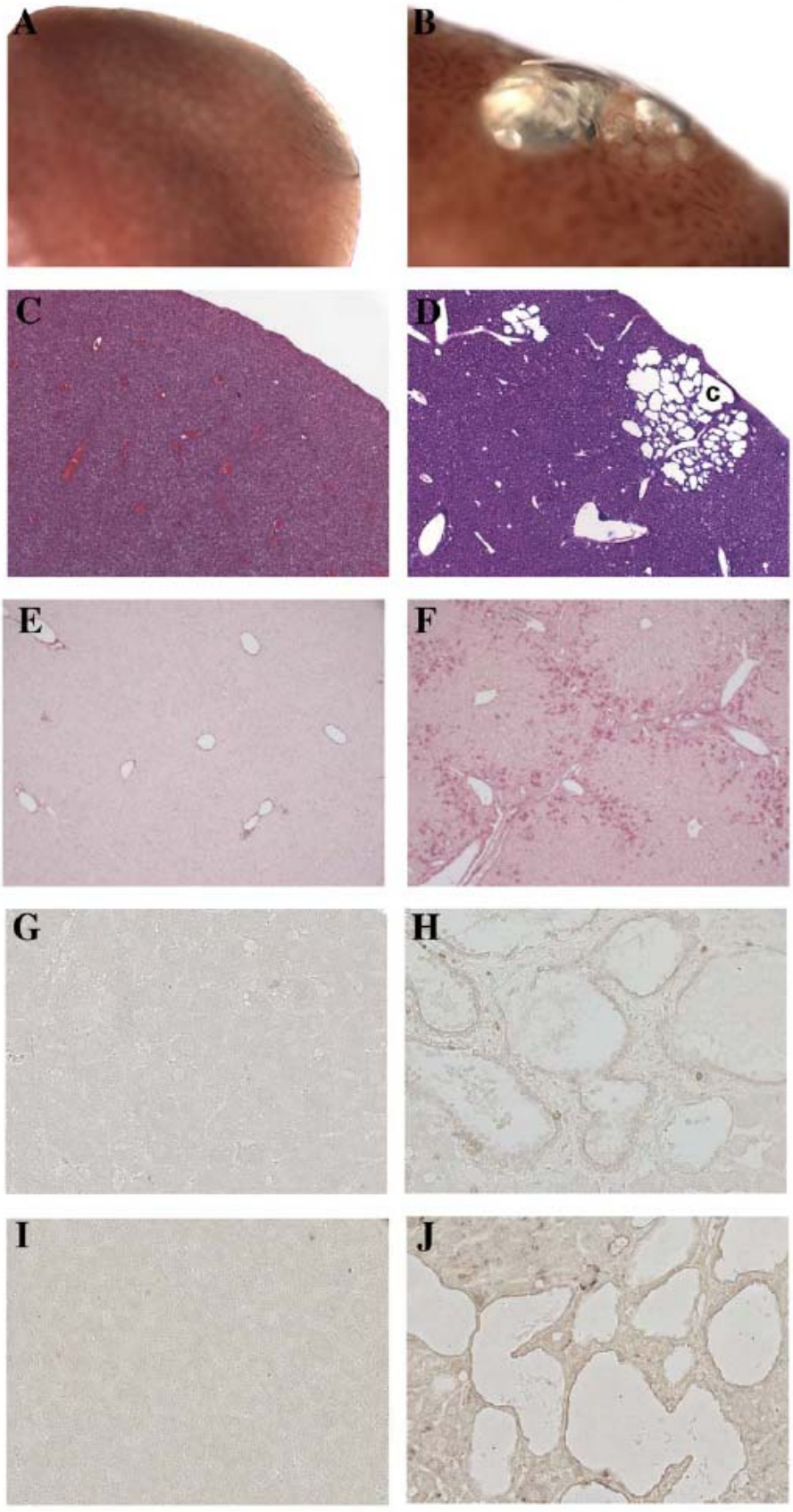

Figure 6

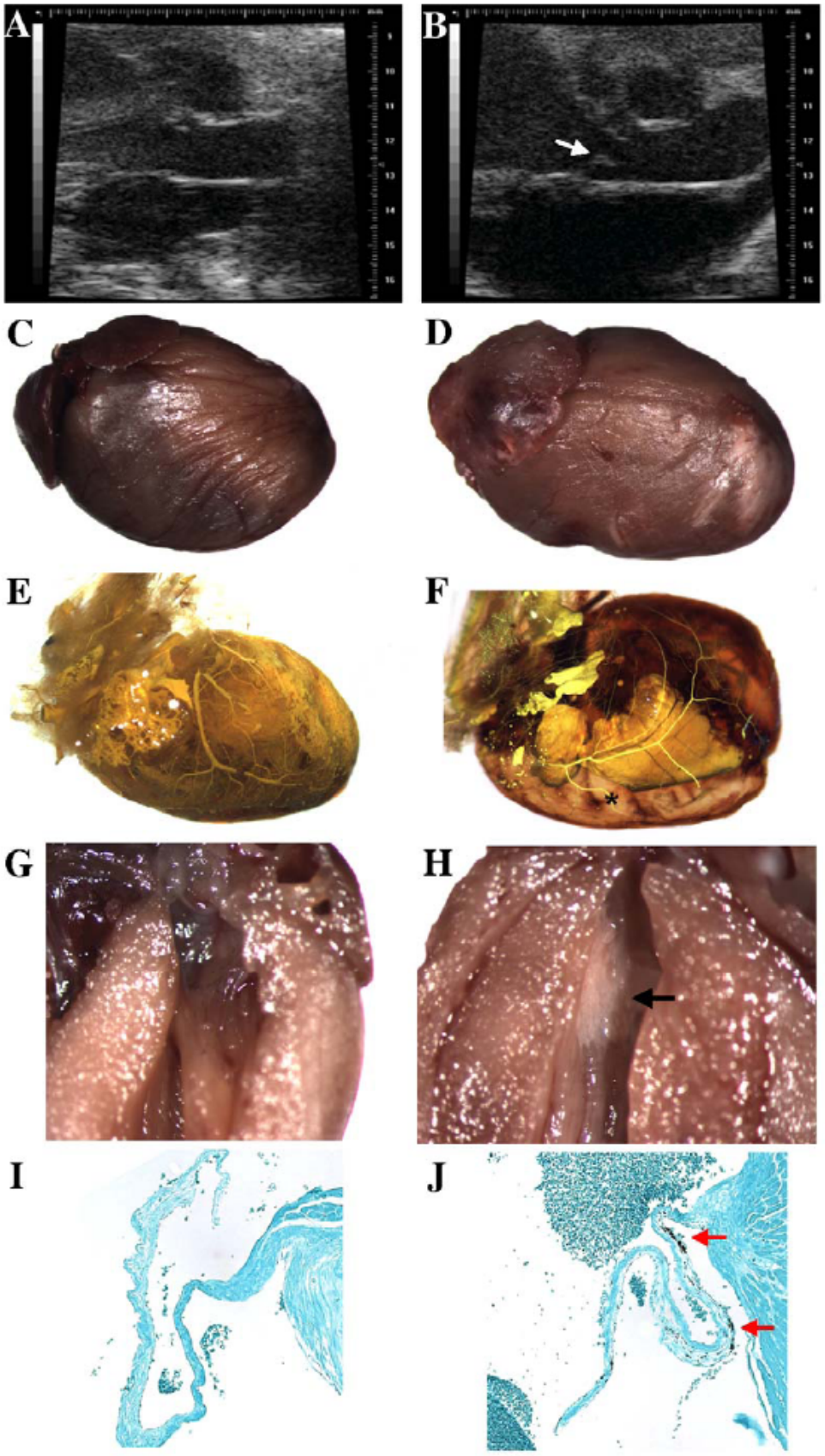

Figure 7

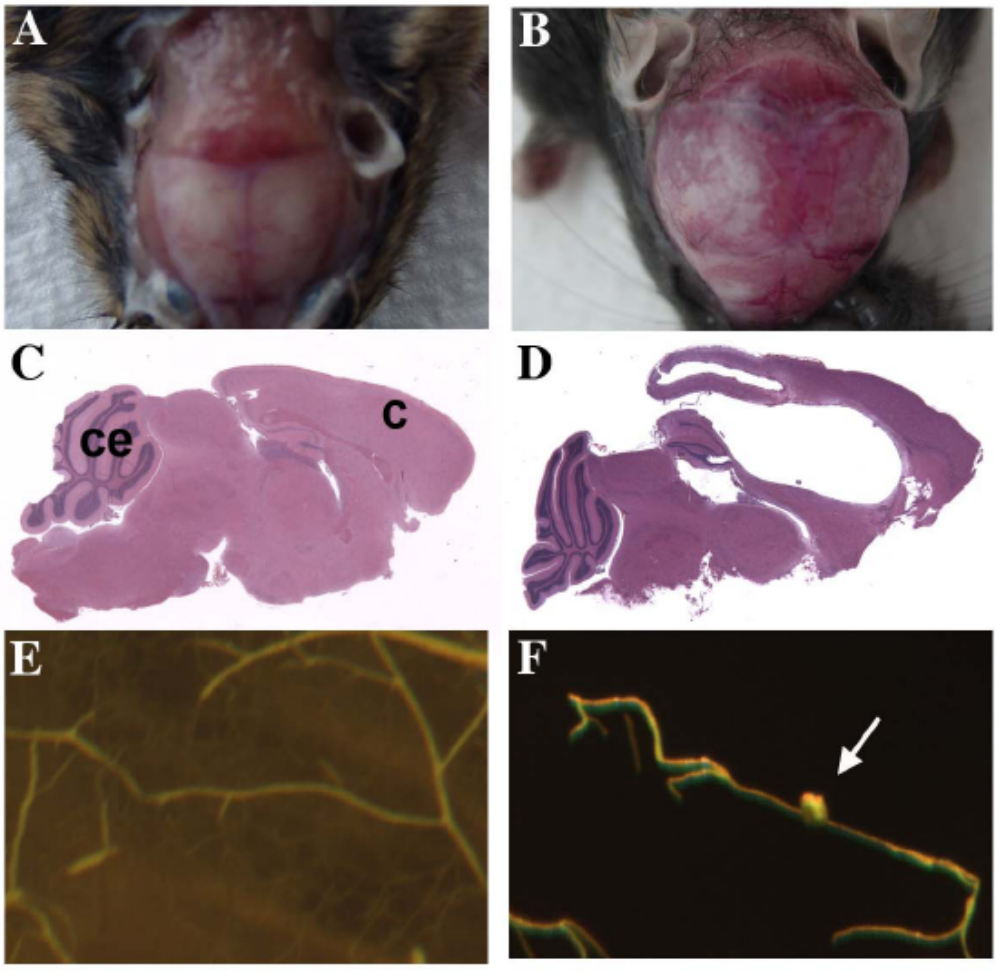

List of Abbreviations

ADPKD	autosomal dominant polycystic kidney disease
Gapdh	glyceraldehyde 3-phosphate dehydrogenase
GPS	G-protein coupled receptor proteolytic site
Pc-1	Pkd1 protein or polycystin-1